

Λ CDM Correctly Predicts Basic Statistics of Galaxies: Luminosity-Velocity Relation, Baryonic Mass-Velocity Relation, and Velocity Function

Sebastian Trujillo-Gomez¹, Anatoly Klypin¹, Joel Primack², and Aaron J. Romanowsky³

¹*Astronomy Department, New Mexico State University, MSC 4500, P.O.Box 30001, Las Cruces, NM, 88000-8001, USA*

²*Department of Physics, University of California at Santa Cruz, Santa Cruz, CA, USA*

³*UCO/Lick Observatory, University of California at Santa Cruz, Santa Cruz, CA 95064 USA*

ABSTRACT

It has long been regarded as difficult if not impossible for a cosmological model to account simultaneously for the galaxy luminosity, mass, and velocity distributions. We revisit this issue using a modern compilation of observational data along with the most advanced large-scale cosmological simulation of dark matter. We find that the standard cosmological model fits – at least on average – all basic statistics of galaxies with circular velocities $V_{\text{circ}} > 50 \text{ km s}^{-1}$ calculated at $\sim 10 \text{ kpc}$ radius. Besides an SDSS-based r -band luminosity function, our primary observational constraint is the luminosity-velocity relation – which generalizes the Tully-Fisher and Faber-Jackson relations in allowing all types of galaxies to be included, and provides a fundamental benchmark to be reproduced by any theory of galaxy formation. We have compiled data for a variety of galaxies ranging from dwarf irregulars to giant ellipticals. The data present a clear monotonic luminosity-velocity relation from $\sim 50 \text{ km s}^{-1}$ to $\sim 500 \text{ km s}^{-1}$, with a bend below $\sim 80 \text{ km s}^{-1}$ and a systematic offset between late- and early-type galaxies. For comparison to theory, we make use of our new Λ CDM “Bolshoi” simulation of dark matter, which has unprecedented mass and force resolution over a large cosmological volume, while using an up-to-date set of initial conditions. We use an abundance-matching technique to assign rank-ordered galaxy luminosities to the dark matter halos, a procedure which automatically fits the empirical luminosity function and provides a predicted luminosity-velocity relation that can be checked against observations. The adiabatic contraction of dark matter halos in response to the infall of the baryons is included as an optional model ingredient. The resulting predictions for the luminosity-velocity relation are in good agreement with the available data on both early-type and late-type galaxies for the magnitude range from $M_r = -14$ to $M_r = -22$. We also compare our predictions for the cold baryon mass of galaxies as a function of circular velocity with the available observations, again finding good agreement except perhaps at the highest V_{circ} . Finally, the predicted circular velocity function is in agreement with the galaxy velocity function from 80 to 400 km s^{-1} , using the HIPASS survey for late-type and SDSS for early-type galaxies. However, in agreement with other recent results, we find that the dark matter halos with $V_{\text{circ}} < 50 \text{ km s}^{-1}$ are much more abundant than observed galaxies with the same V_{circ} .

Subject headings: cosmology: theory — dark matter — galaxies: halos — galaxies: structure

1. Introduction

The cosmological constant + cold dark matter (Λ CDM) model is the reigning paradigm of struc-

ture formation in the universe. The presence of large amounts of dark mass in the surroundings of galaxies and within galaxy clusters has been established firmly using dynamical mass estimates

that include spiral galaxy rotation curves, velocity dispersions of galaxies in clusters and x-ray emission measurements of the hot gas in these systems, as well as strong and weak lensing of background galaxies. The Λ CDM model also correctly predicts the details of the temperature and polarization of the cosmic background radiation (Komatsu et al. 2010). A few issues remain where the model and the observations are either hard to reconcile or very difficult to compare (Primack 2009). Examples of this are the so-called missing satellites problem (Klypin et al. 1999; Moore et al. 1999; Bullock et al. 2000; Willman et al. 2004; Macciò et al. 2010) and the cusp/core nature of the central density profiles of dwarf galaxies (Flores & Primack 1994; Moore 1994; de Blok & McGaugh 1997; Valenzuela et al. 2007; Governato et al. 2010; de Blok 2010).

An outstanding challenge for the Λ CDM model that we address here is to reproduce the observed abundance of galaxies as a function of their overall properties such as dynamical mass, luminosity, stellar mass, and morphology, both nearby and at higher redshifts. A successful cosmological model should produce agreement with various observed galaxy dynamical scaling laws such as the Faber-Jackson (Faber & Jackson 1976) and Tully-Fisher (Tully & Fisher 1977) relations.

Making theoretical predictions for properties of galaxies that can be tested against observations is difficult. While dissipationless simulations can provide remarkably accurate predictions of various properties of dark matter halos, they do not yet make secure predictions about what we actually observe – the distribution and motions of stars and gas. We need to find a common ground where theoretical predictions can be confronted with observations. In this paper we use three statistics to compare theory and observations: (a) the luminosity - circular velocity (LV) relation, (b) the baryonic Tully-Fisher relation (BTF), and (c) the circular velocity function (VF).

In all three cases we need to estimate the circular velocity (a metric of dynamical mass) at some distance from the center of each dark matter halo that hosts a visible galaxy. Unfortunately, theory cannot yet make accurate predictions for the central regions of galaxies because of uncertain baryonic astrophysics. As a compromise, we propose to use the distance of 10 kpc. Measurements of

rotational or circular velocities of galaxies either exist for this distance or can be approximated by extrapolations. At the same time, theoretical predictions at 10 kpc are also simplified because they avoid complications of central regions of galaxies.

Our LV relation is a close cousin of the Tully-Fisher (TF) relation and, indeed, we will use some observational results used to construct the normal Tully-Fisher relation. However, there are substantial differences between the TF and the LV relations. The normal Tully-Fisher relation tells us how quickly spiral disks rotate for given luminosity. The rotation velocity is typically measured at 2.2 disk scale lengths (e.g., Courteau et al. 2007), where the baryons contribute a substantial fraction of the mass. Instead, at the 10 kpc radius used here for the LV relation, the dark matter is the dominant contribution to the mass in all but the largest galaxies. More importantly, the LV relation is not only for spiral galaxies; it is for all morphological types. Thus, *the LV relation is the relation between the galaxy luminosity and the total mass inside the 10 kpc fiducial radius.*

In order to make theoretical predictions for the LV relation, we need to estimate the luminosity of a galaxy expected to be hosted by a (sub)halo. There are different ways to make those predictions. Cosmological N -body+gasdynamics simulations will eventually be an ideal tool for this. However, simulations are still far from achieving the resolution and physical understanding necessary to correctly model the small scale physics of galaxy formation and evolution. Early simulations had problems reproducing the TF relation (e.g., Navarro & Steinmetz 2000). Eke et al. (2001) could reproduce the slope of the TF relation, but created disks that were too faint by about 0.5 magnitudes in the I -band for any given circular velocity. Recently the situation has improved. For example, Governato et al. (2007) produced disk galaxies spanning a decade in mass that seem to fit both the I -band TF relation and the baryonic TF relation very well, as well as the observed abundance of Milky Way-type satellites. Agertz et al. (2010), using an adaptive mesh hydrodynamics code and a different sub-grid star formation prescription, have also shown that a Milky Way-type galaxy can form naturally in Λ CDM.

Making predictions for a large ensemble of simulated galaxies is yet another challenge. Semi-

analytical models (SAMs) are a way to make some progress in this direction. These models have the advantage of producing large-number galaxy statistics. They typically include many free parameters controlling the strength of the various processes that affect the build-up of the stellar population of a galaxy (i.e., cooling, star formation, feedback, starbursts, AGNs, etc.). Unfortunately, these normalizing parameters can be difficult to constrain observationally (e.g., Somerville & Primack 1999; Benson & Bower 2010). The models aim to reproduce the observed number distributions of galaxies as a function of observables such as luminosity, stellar mass, cold gas mass, and half-light radius, along with scaling laws such as the Tully-Fisher relation and the metallicity-luminosity relation.

Early SAMs suffered from serious defects. The models of Kauffmann et al. (1993) were normalized using the observed TF relation zero-point, which resulted in a luminosity function with a very steep faint-end. On the other hand, models such as those of Cole et al. (1994) were normalized to reproduce the observed “knee” in the LF but this resulted in a large offset in the TF relation zero-point. Later models have shown moderate success in reproducing either the luminosity function (Benson et al. 2003) or the TF relation (Somerville & Primack 1999), but it has been difficult to match both simultaneously when rotation curves are treated realistically (Cole et al. 2000). Benson et al. (2003) used a combination of disk and halo reheating to obtain reasonable agreement with the observed LF except at the faint end, where they still overpredict the number of dwarf galaxies. If the WMAP 5-year cosmology (Komatsu et al. 2009) were used, their models would also produce too many very bright galaxies. The TF relation they obtain has the correct slope but their disks are too massive at any given luminosity. Most recently, Benson & Bower (2010) used a sophisticated version of their GALFORM semi-analytic model to obtain sets of parameters that minimize the deviations from twenty one observational datasets including the LFs in several bands and at different redshifts, the TF relation, the average star formation rate as a function of redshift, clustering and metallicities among many others. Not surprisingly, even their best model has difficulty fitting such a large number of simu-

taneous constraints. In particular, the LF in the K band overpredicts the number of dwarf galaxies by almost an order of magnitude at the faint end, while the LFs at high redshift consistently overpredict the abundance of all galaxies. In addition, the halos they obtain contain too many satellite galaxies, resulting in too strong a galaxy two-point correlation in the one-halo regime. The Tully-Fisher relation of their best fit model also shows a systematic offset of about $20 - 40 \text{ km s}^{-1}$ towards higher circular velocities for given luminosity when compared to observations.

Recent high-resolution N -body cosmological simulations such as Springel et al. (2005); Klypin et al. (2010) have volumes large enough to obtain the mass function of dark matter (DM) halos, but there is no direct way to compare it to observational measurements of the luminosity or stellar mass functions of galaxies. A new technique recently emerged that allows us to bridge the gap between dark matter halos and galaxies. It is called abundance-matching (Kravtsov et al. 2004; Tasitsiomi et al. 2004; Vale & Ostriker 2004; Conroy et al. 2006; Conroy & Wechsler 2009; Guo et al. 2010). Abundance-matching resolves the issue of connecting observed galaxies to simulated dark matter (DM) halos by setting a one-to-one correspondence between red-band luminosity and dynamical mass: more luminous galaxies are assigned to more massive halos. By construction, it reproduces the observed luminosity function. It also reproduces the scale dependence of galaxy clustering over a range of epochs (Conroy et al. 2006; Guo et al. 2010). When abundance matching is used for the observed stellar mass function (Li & White 2009), it gives a reasonably good fit to the lensing results (Mandelbaum et al. 2006) on the relation between the stellar mass and the virial mass (Guo et al. 2010). Guo et al. (2010) also tried to reproduce the observed relation between the stellar mass and the circular velocity with partial success: there were deviations in both the shape and the amplitude. At circular velocities $V_c = 100 - 150 \text{ km s}^{-1}$ the predicted circular velocity was $\sim 25\%$ lower than the observed one. They argued that the disagreement is likely due to the fact that they did not include the effect of baryons. Below we show that this is indeed the case.

The paper is structured in the following way.

Section 2 describes in detail the observational samples used to compare with the results of our analysis. Section 3 briefly describes our new Bolshoi simulation (Klypin et al. 2010) and compares it to other large cosmological simulations. In section 4 we describe some characteristics of dark matter halos. Section 5 describes the abundance-matching method used to relate observed galaxies to the DM halos in the Bolshoi simulation and explains the procedure used to measure key quantities such as the circular velocity for these model galaxies. Section 2 describes in detail the observational samples used to compare with the results of our analysis. Section 6 shows the LV relation, the baryonic Tully-Fisher relation, and the galaxy circular velocity function obtained using our procedure and compares them to the observations described in Section 2. A brief comparison with related results in the literature is given in Section 7. Section 8 presents a discussion and a brief summary of our results.

2. Observational Data

2.1. Late-type galaxies

We use different observational samples to construct the LV relation for real galaxies. Springob et al. (2007) compiled a template I -band Tully-Fisher sample of 807 spiral galaxies of types Sa-Sd in order to calibrate distances to ~ 4000 galaxies in the local universe. Their template galaxies were chosen to be members of nearby clusters in order to minimize distance errors. Their photometry contains distance uncertainties so the scatter should be taken cautiously and only as an upper limit to the intrinsic TF scatter. To obtain the circular velocities they use HI line synthesis observations or optical $H\alpha$ rotation curves when these are not available. The maximum circular velocity is obtained by using a model fit to the observed profiles. From the sample we selected galaxies with redshifts larger than 1000 km s^{-1} to minimize peculiar motion uncertainties. In addition, we included only galaxies with inclinations $i > 35$ deg to minimize velocity errors due to projection effects. Since the authors correct for the effects of turbulence by subtracting 6.5 km s^{-1} linearly from the velocity widths, it was necessary to de-correct them by adding this term back in to obtain the true circular velocities

The Pizagno et al. (2007) sample was selected from the Sloan Digital Sky Survey (SDSS) (York et al. 2000). It is one of the most complete and unbiased samples available of $H\alpha$ rotation curves of disk galaxies of all morphological types and was studied in an attempt to accurately measure the intrinsic scatter in the TF relation. Luminosities are taken from the SDSS r -band photometry, yielding the best match with the luminosities assigned to our model galaxies. From their sample we selected only galaxies with axis ratios $b/a < 0.5$ (122 galaxies) and used the asymptotic value of the rotation velocity they obtained using a functional fit to the rotation curves.

The sample of Blanton et al. (2008) is comprised of only isolated galaxies with high inclinations. The HI galaxy sample used by Sakai et al. (2000) was selected to have small scatter for the purpose of distance calibration. It is important to note that while the fit shown here minimizes both the errors in rotation velocity and in luminosity, it may be artificially shallow due to selection effects.

In order to test the predictions of Λ CDM with the largest dynamical range possible, we included in our comparison the latest Tully-Fisher dwarf galaxy sample studied by Geha et al. (2006). Their sample consists of about 110 late-type galaxies with luminosities measured in the r -band and rotation velocities measured using HI emission. Out of their full sample we selected only those galaxies that had high inclinations ($b/a < 0.5$) and errors in the measurement of the velocity width of less than 10%.

Different assumptions about galaxy colors had to be made in order to convert the different observational samples to the $0.1r$ -band measurements we chose for our model. In order to convert the I -band luminosities measured by Springob et al. (2007) to the r -band, we cross-referenced their data with the sample of Pizagno et al. (2007) and used the median $(r - I)$ colors of the galaxies present in both catalogs. To convert from the R -band magnitudes of Sakai et al. (2000) to the SDSS $0.1r$ -band we used the transformation equations obtained by Lupton (2005) along with the typical $0.1(r - i)$ color of disk galaxies in the SDSS sample studied by Blanton et al. (2003a). In addition, for redshift zero data sets, the k-correction given in Blanton et al. (2003b) was used to convert from $z = 0$ to $z = 0.1$ photometric bands.

Lastly, since the obscuring effect of dust extinction as a function of disk inclination is corrected for in Tully-Fisher samples but not in observed LF estimates, we had to de-correct the luminosities of the spiral galaxies in all of the TF samples we use for comparison with our model galaxies. To do so, we estimated and added the median extinction in the r -band as a function of rotation velocity using the method employed by Pizagno et al. (2007). This correction is ~ 0.4 mag at the bright end of LF declining to ~ 0.3 mag for $V_{\text{circ}} \approx 100 \text{ km s}^{-1}$.

2.2. Early-type galaxies

We also include bulge-dominated early-type galaxies (ellipticals and lenticulars) in the LV relation, again measuring the circular velocity at our fiducial 10 kpc radius. The circular velocity in this case is used not as a measure of rotation but merely as a probe of the mass profile, further justifying the use of the term “LV relation” instead of TF relation. Using early-type galaxies allows us to probe closer to the mass regime where the abundance of DM halos drops exponentially (i.e., the knee of the velocity distribution function) and also allows for study of halo-galaxy relations without regard to the details of the evolution of the stellar populations within them.

Because of the challenges of both observing and modeling early-type galaxies, so far there exists no comprehensive set of mass measurements for them akin to the spiral galaxy samples. Instead, we compile a set of high-quality LV estimates for individual galaxies from the literature.

To provide the necessary LV data for nearby elliptical and lenticular galaxies, we searched the literature for high-quality mass measurements at ~ 10 kpc radii. A variety of different mass tracers were used including hot X-ray gas, cold gas disks and rings, and kinematics of stars, globular clusters, and planetary nebulae. We required the mass models to incorporate spatially-resolved temperature profiles in the case of X-ray studies, and to take some account of orbital anisotropy effects in the case of dynamics. We also used only those cases where V_{10} was constrained to better than $\sim 15\%$. We make no pretense that this is a systematic, unbiased, or especially accurate sample of early-type masses, noting simply that it is preferable to ignoring completely this class of galaxies which dominates the bright end of the luminosity

function.

We find in comparing to central velocity dispersions σ_0 taken from HyperLeda (Paturel et al. 2003), that the scaling $v_{10} \simeq \sqrt{2}\sigma_0$ works very well on average, suggesting near-isothermal density profiles over a wide range of galaxy masses. It is far easier to measure σ_0 observationally than v_{10} , motivating the use of the former as a proxy for the true V_{circ} which is more robustly predicted by theory. The $\sim 15\%$ scatter that we find in the σ_0 – v_{10} relation is relatively small, but it is beyond the scope of this paper to consider the potential systematics of using σ_0 as a proxy. We will use V_{10} for the LV analysis in this paper.

For the luminosities, we make use of the total B -band apparent magnitudes from the RC3 (de Vaucouleurs et al. 1991), corrected for Galactic extinction. To correct to $^{0.1}r$ magnitudes, we use typical colors $B - r = 1.34$ based on Peletier et al. (1990) and Hill et al. (2010), and then k-correct as discussed in the main text. For the distances (required both for absolute magnitudes and for choosing the circular velocity measurement radii in kpc), we use as a first choice the estimates from surface brightness fluctuations (Jensen et al. 2003), and otherwise the recession velocity with $h = 0.7$.

There is an additional complication with the photometry, which is that for the abundance matching in this paper, Petrosian magnitudes and stellar masses were drawn from the SDSS. These values will be accurate enough for the disk galaxies, but for the early-types, they systematically underestimate the luminosities (Strauss et al. 2002). With the alternatives of either correcting the luminosity and stellar-mass inputs at the abundance matching step (cf. Appendix A of Guo et al. 2010), or correcting the LV data for local galaxies, we have opted for the latter. Although this choice loses some of the physical significance of the magnitudes plotted, as long as there is consistency between the magnitude conventions used in the abundance-matching and local-data steps, the comparisons between the models and data should remain fair. To correct the local data to Petrosian magnitudes, we increase the RC3 photometry (presumed to be equivalent to $R^{1/4}$ -based values) by 0.2 mag. This correction will be too large for the S0s, and too small for the brightest ellipticals with their extended sur-

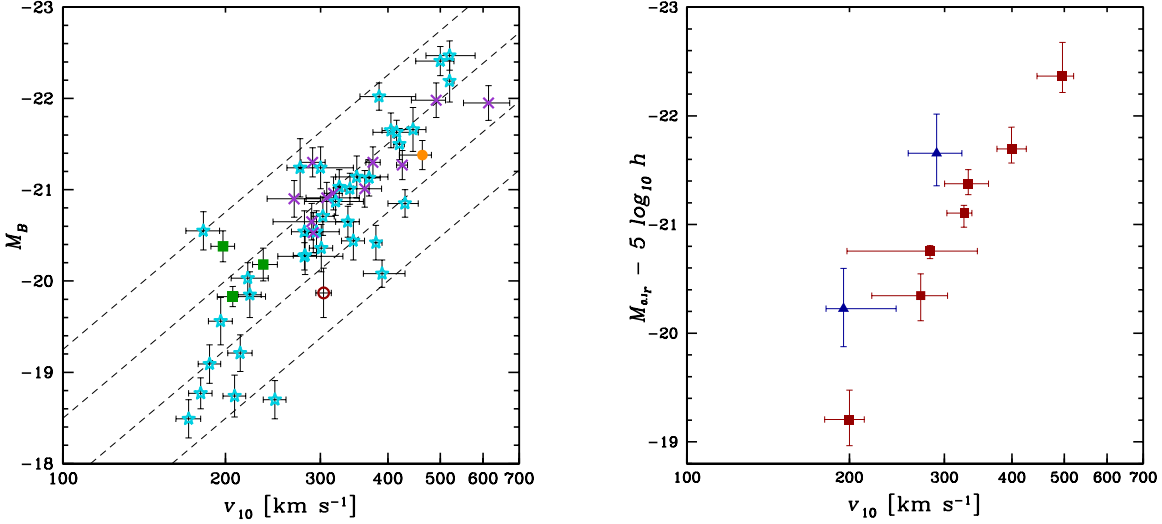


Fig. 1.— Absolute magnitude versus circular velocity at 10 kpc, for early- and late-type galaxies. *Left panel*: Individual data points for early-type galaxies, using B -band magnitudes at $z \sim 0$. Symbols indicate the mass probe used: stellar kinematics (*light blue stars*), X-ray gas (*purple triangles*), planetary nebula kinematics (*green squares*), globular cluster kinematics (*orange filled circle*), and cold gas rings and disks (*red open circle*). Dashed lines show B -band dynamical mass-to-light ratios of $M/L_B = 3, 6, 12$, and 24 (*top to bottom*); for comparison, early-type galaxies are expected to have stellar $M/L_B \sim 2.4\text{--}3.1$. *Right panel*: Binned averages, with error bars showing the scatter in each bin; blue triangles (spirals in Williams et al. 2009) and red squares show the late- and early-types, respectively.

face brightness profiles and high Sérsic indices (cf. Graham et al. 2005; Lauer et al. 2007), but degrading the photometry to Petrosian magnitudes on a galaxy-by-galaxy basis is beyond the scope of the current paper.

The local data for 52 individual early-type galaxies are presented in Figure 1 (left). Dashed lines show B -band dynamical mass-to-light ratios of $M/L_B = 3, 6, 12$, and 24 ; for comparison, early-type galaxies with typical colors ($B - V \sim 0.85\text{--}1.0$) are expected to have stellar $M/L_B \sim 2.4\text{--}3.1$ for a Chabrier IMF (e.g., Fig. 18 of Blanton & Roweis (2007)). A data table is provided in electronic format online. There is no obvious systematic difference between the results from different mass tracers. The galaxies appear to trace a fairly tight LV sequence, except around the L^* luminosity, where there are a few galaxies whose circular velocities appear to be fairly high or low. The low- V_{10} galaxies include NGC 821 and NGC 4494, which were previously suggested as having a “dearth of dark matter”

(Romanowsky et al. 2003), and as implying a dark matter “gap” with respect to X-ray bright ellipticals (Napolitano et al. 2009). The present compilation suggests that the galaxy population in the local universe may fill in this gap, although further work will be needed to understand the scatter.

In the right panel of Figure 1 we include for direct comparison the spiral galaxies (blue triangles) with masses based on stellar dynamics from Williams et al. (2009). Magnitudes have been shifted to r -band using typical blue-cloud and red-sequence $B-r$ colors from (Hill et al. 2010), and k-corrected to $z = 0.1$. After ~ 1 mag corrections for internal extinction, the spirals are brighter than the early-types by ~ 0.5 mag at fixed V_{10} .

When using the data of Williams et al. (2009) for S0 galaxies, we corrected stellar mass-to-light ratios M/L_K in K -band so that they do not exceed $M/L_K = 1$, to be compatible with population synthesis constraints (Maraston 2005). This affects circular velocities (reducing typically by 10–20%) of only a small fraction of galaxies.

2.3. Observational LV relation

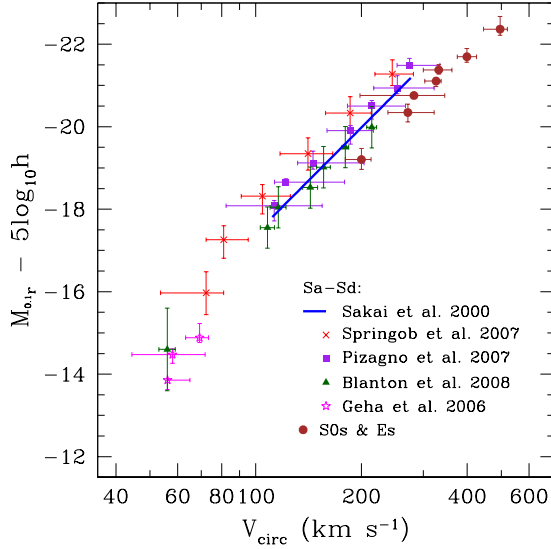


Fig. 2.— The r -band luminosity versus circular velocity for several observational samples across different morphological types. All absolute magnitudes were transformed to the SDSS r -band at redshift $z = 0.1$.

Figure 2 shows the combined LV relation for galaxies of different types: from Magellanic dwarfs with $V_{\text{circ}} \approx 50 \text{ km s}^{-1}$ to giant ellipticals with $V_{\text{circ}} \approx 500 \text{ km s}^{-1}$. The LV relation is not a simple power-law. Dwarf galaxies show a tendency to have lower luminosities as compared with a simple power-law extrapolation from brighter magnitudes. There is a clear sign of bimodality at the bright end of the LV relation with early type galaxies having $\sim 20\%$ circular velocities as compared with the spiral galaxies with the same r -band magnitude.

3. The Bolshoi simulation

The Bolshoi simulation was run using the following cosmological parameters: $\Omega_{\text{matter}} = 0.27$, $h = 0.70$, $\sigma_8 = 0.82$, $\Omega_{\text{bar}} = 0.0469$, $n = 0.95$. These parameters are compatible with the WMAP seven-year data (WMAP7) (Jarosik et al. 2010) and with WMAP5 combined with Baryon Acoustic Oscillations and Type 1a Supernova data (Hinshaw et al. 2009; Komatsu et al. 2009; Dunkley et al. 2009). The

Bolshoi parameters are in excellent agreement with the SDSS maxBCG+WMAP5 cosmological parameters (Rozo et al. 2009) and with cosmological parameters from WMAP5 plus recent X-ray cluster survey results (Klypin et al. 2010).

The Millennium simulation (Springel et al. 2005, MS-I) has been the basis for many studies of the distribution and statistical properties of dark matter halos and for semi-analytic models of the evolving galaxy population. However, it is important to appreciate that this simulation and the more recent Millennium-II simulation (Boylan-Kolchin et al. 2009, MS-II) used the first-year (WMAP1) cosmological parameters, which are rather different from the current estimates of the parameters. The main difference is that the Millennium simulations used a substantially larger amplitude of perturbations than Bolshoi. Formally, the value of σ_8 used in the Millennium simulations is more than 3σ away from the WMAP5+BAO+SN value and nearly 4σ away from the WMAP7+BAO+ H_0 value. However, the difference is even larger on galaxy scales because the Millennium simulations also used a larger tilt $n = 1$ of the power spectrum.

The Bolshoi simulation uses a computational box $250 h^{-1} \text{ Mpc}$ across and $2048^3 \approx 8$ billion particles, which gives a mass resolution (one particle mass) of $m_1 = 1.35 \times 10^8 h^{-1} M_\odot$. The force resolution (smallest cell size) is physical (proper) $1 h^{-1} \text{ kpc}$. For comparison, the Millennium-I simulation had force resolution (Plummer softening length) $5 h^{-1} \text{ kpc}$ and the Millennium-II simulation had $1 h^{-1} \text{ kpc}$. The Bolshoi simulation was run with the Adaptive-Refinement-Tree (ART) code, which is an Adaptive-Mesh-Refinement (AMR) type code. A detailed description of the code is given in Kravtsov et al. (1997); Kravtsov (1999). We refer the reader to the main Bolshoi paper (Klypin et al. 2010) for more details specific to the use of the code for the simulation.

We use a parallel (MPI+OpenMP) version of the Bound-Density-Maxima (BDM) algorithm to identify halos in Bolshoi (Klypin & Holtzman 1997). BDM does not distinguish halos and subhalos – they are treated in the same way. The code locates maxima of density in the distribution of particles, removes unbound particles, and provides several statistics for halos including virial mass and radius, and maximum circular velocity.

We use the virial mass definition M_{vir} that follows from the top-hat model in the expanding Universe with a cosmological constant. We define the virial radius R_{vir} of halos as the radius within which the mean density is the virial overdensity times the mean universal matter density $\rho_{\text{m}} = \Omega_{\text{m}}\rho_{\text{crit}}$ at that redshift. Thus, the virial mass is given by

$$M_{\text{vir}} \equiv \frac{4\pi}{3} \Delta_{\text{vir}} \rho_{\text{m}} R_{\text{vir}}^3. \quad (1)$$

For our set of cosmological parameters, at $z = 0$ the virial radius R_{vir} is defined as the radius of a sphere enclosing average overdensity equal to $\Delta_{\text{vir}} = 360$ times the average matter density. The overdensity limit changes with redshift and asymptotically goes to 178 for high z . Different definitions are also found in the literature. For example, the often used overdensity 200 relative to the *critical* density gives mass M_{200} , which for Milky-Way-mass halos is about 1.2-1.3 times smaller than M_{vir} . The exact relation depends on halo concentration.

Overall, there are about 10 million halos in Bolshoi (8.8×10^6 at $z = 0$, 12.3×10^6 at $z = 2$, 4.8×10^6 at $z = 5$). The halo catalogs are complete for halos with $V_{\text{circ}} > 50 \text{ km s}^{-1}$ ($M_{\text{vir}} \approx 1.5 \times 10^{10} h^{-1} M_{\odot}$). In order to track evolution of halos over time, we find and store the 50 most bound particles. Together with other parameters of the halo (coordinates, velocities, virial mass, and circular velocity) the information on most bound particles is used to identify the same halos at different moments of time. The procedure of halo tracking starts at $z = 0$ and goes back in time. The final result is the history (*track*) of the major progenitor of a given halo.

4. DM halos: definitions and characteristics

We distinguish between two types of halos. A halo can be either distinct (not inside the virial radius of a larger halo), or a subhalo if it is inside of a larger halo. For both distinct halos and subhalos, the BDM halo finder provides the maximum circular velocity

$$V_{\text{circ}} = \sqrt{\frac{GM(< r)}{r}} \Big|_{\text{max}}. \quad (2)$$

Throughout this paper we will use term *circular velocity* to mean maximum circular velocity.

As the main characteristic of the DM halos we use their circular velocity V_{circ} . There are advantages to using V_{circ} as compared with the virial mass M_{vir} . The virial mass is a well defined quantity for distinct halos, but it is ambiguous for subhalos. It strongly depends on how a particular halo-finder code defines the truncation radius and removes unbound particles. It also depends on the distance to the center of the host halo because of the effects of tidal stripping. Instead, the circular velocity is less prone to those complications. The main motivation for using V_{circ} in this work is that it is more closely related to the properties of the central regions of halos and, thus, to galaxies hosted by those halos. For example, for a Milky-Way type halo the radius of the maximum circular velocity is about 40 kpc (and V_{circ} is nearly the same at 20 kpc), while the virial radius is about 300 kpc. In addition, the virial mass of a DM halo is not an easily observable quantity and this further limits its use for comparison of simulations with observations.

Tidal stripping of subhalos can lead to significant mass loss in the periphery of the halo. The net effect at redshift zero of the complex merger and interaction history of each halo is a decrease in the maximum circular velocity, compared to its peak value over the entire history of the halo. The galaxy residing in the central region of the halo should not experience much of the stripping and should preserve most of its mass inside optical radius (e.g., Conroy et al. 2006). Following this argument, the initial total mass distribution and rotation profile of the halo are frozen at the moment before the halo is accreted and starts to experience the stripping. We refer to this circular velocity as V_{acc} . In practice we find the peak circular velocity of the halo over its entire history.

5. Connecting galaxies and DM halos

To investigate the statistics of galaxies and their relation to host DM halos as predicted by the Λ CDM model, we predicted the properties of our model galaxies using the following procedure:

1. Using the merger tree of each DM halo and subhalo, obtain $V_{\text{acc}} =$ the peak value of the circular velocity over the history of the halo (this is typically the maximum circular velocity of the halo when the halo is first

accreted). Perform abundance matching of the velocity function of the halos to the LF of galaxies to obtain the luminosity of each model galaxy.

2. Perform abundance matching of the velocity function to the stellar mass function of galaxies to obtain the stellar mass of each model galaxy.
3. Use the observed gas-to-stellar mass ratio as a function of stellar mass to assign cold gas masses to our model galaxies. The stellar mass added to the cold gas mass becomes the total baryonic mass.
4. Using the density profiles of the DM halos, obtain the circular velocity at 10 kpc (V_{10}) from the center of each halo. Multiply the DM mass, as it comes from simulations, by the factor $(1 - f_{\text{bar}})$, where f_{bar} is the cosmological fraction of baryons. This is the dark-matter-only contribution.¹ Add the contribution to V_{10} of the baryon mass from step 3 assuming it is enclosed within a radius of 10 kpc.
5. Implement the correction to V_{10} due to the adiabatic contraction of the DM halos due to the infall of the baryon component to the center.

We now explain each of the above 5 steps in detail.

Using the key assumption that halos with deeper potential wells become sites where more baryons can gather to form larger and more luminous galaxies, we ranked our halos and subhalos using their V_{circ} , and starting from the bright end of the r -band LF, assigned luminosities to each according to their space density using the prescription found in Conroy et al. (2006). In other words, we found the unique one-to-one correspondence that would match the halo velocity function with the luminosity function of observed galaxies. Of course, this is a simplifying approximation. It does not discriminate between blue (star-forming) and red (quenched) galaxies, for example.

¹Recall that the Bolshoi simulation was run for a dissipationless cosmic density $\Omega_m = \Omega_{\text{dm}} + \Omega_{\text{bar}} = 0.27 = \Omega_{\text{dm}}(1 + f_{\text{bar}})$.

In this paper we use the triple-Schechter fit to the r -band galaxy LF measurement of Montero-Dorta & Prada (2009) obtained from the SDSS Data Release 6 (DR 6) galaxy sample. Since the median redshift of the SDSS DR6 sample is ≈ 0.1 (Blanton et al. 2003a), all our subsequent results will be shown in $^{0.1}r$ -band magnitudes.

As a test, we also consider a LF with a steeper slope at low-luminosities. Blanton et al. (2005) obtained the SDSS LF including dwarfs as faint as $M_r = -12$ and investigated surface brightness completeness at the faint end of the LF. To quantify the effect of including low surface brightness galaxies in our model (those with Petrosian half-light r -band surface brightness greater than 24.0), we increased the abundance of bright galaxies in the Blanton et al. (2005) LF to match the Montero-Dorta & Prada (2009) LF at the bright end while keeping the steep faint-end slope ($\alpha = -1.34$) measured by Blanton et al. (2005). Their steeper value of the faint-end slope was obtained by weighting the abundance of each galaxy by its estimated surface brightness completeness. The modified LF produces 60% more galaxies at $M_r \sim -16$ and over a factor of 2.5 more galaxies at $M_r \sim -13$. Using this LF to perform the abundance matching increases the luminosity of galaxies assigned to small DM halos, steepening the faint end of the LV relation.

It is important to note that we assume that each dark matter halo or subhalo must contain a galaxy with a detectable luminous component (for the SDSS r -band this requires galaxies to be detectable in visible wavelengths) and this component must evolve in a way that guarantees its detectability at $z = 0$. Since the effective volume surveyed by SDSS DR6 at $z < 0.3$ is comparable to the volume of the Bolshoi simulation, we expect the statistics of the halo population to be comparable to those of the observed galaxies all the way up to the large mass/luminosity tail of the distributions. Even though Bolshoi contains a factor of ~ 1.8 more objects than the sample of Montero-Dorta & Prada (2009), abundance matching is mostly insensitive to uncertainties in the high-luminosity tail of the LF.

5.1. The circular velocity of galaxies inside halos including baryons

The next step is to separate the DM and baryon components in each halo and allow the baryons to dissipatively sink to the centers of the DM halos. We assume for simplicity that there is a radius at which we could consider most of the “cold” baryons (stars and cold gas) to be enclosed, with only dark matter present beyond that point.

This cold baryon component has been observed to comprise only a small fraction of the cosmic abundance of baryons; in other words, the cold baryon fraction $f_{\text{bar}} \equiv M_{\text{bar}}/(M_{\text{DM}} + M_{\text{bar}})$ in galaxies is much lower (Fukugita et al. 1998; Fukugita & Peebles 2004) than $\Omega_{\text{bar}}/\Omega_{\text{matter}} = 0.17$ (Komatsu et al. 2009). We resort to the observations and use the galaxy stellar mass function obtained from SDSS DR7 by Li & White (2009), who estimate stellar masses using five-band SDSS photometry assuming the universal IMF of Chabrier (2003). These masses are consistent with those estimated using single-color and spectroscopic techniques (Li & White 2009).

Using the same procedure described above for the luminosity function, we abundance-matched the halos in Bolshoi to the galaxies in the SDSS DR7 starting from the high stellar mass end until reaching our completeness limit at $V_{\text{circ}} = 50 \text{ km s}^{-1}$, obtaining stellar masses for each galaxy. Since dwarfs can have most of their baryons in the gas phase instead of in stars (Baldry et al. 2008), we added to each model galaxy the total gas mass obtained using a parameterization of the observed gas mass fraction as a function of stellar mass found by Baldry et al. (2008). This includes the total cold atomic and molecular gas found in the disk only. The gas-to-stellar mass ratio f_{gas} depends on stellar mass and it is the largest for dwarfs. For example, $f_{\text{gas}} \approx 4 - 5$ for galaxies with $M_* = 10^8 M_\odot$. It declines to $f_{\text{gas}} \approx 0.25(0.1)$ for galaxies with $M_* = 10^{10}(10^{11}) M_\odot$. It should be even smaller for ellipticals and S0s. It should be noted that, when it comes to corrections to V_{circ} , the gas plays a minor role. It only becomes important when we consider the baryonic Tully-Fisher relation.

Lastly, we add the stellar and cold gas masses for each model galaxy and obtain the correction to the circular velocity of the pure DM halo at a

radius enclosing the total baryonic mass. We set this value to 10 kpc for all the halos in our sample. In the case of dwarf galaxies this should be a good approximation to the maximum circular velocity since their rotation curves rise much more slowly and in some cases they peak beyond the optical radius (Courteau 1997). Our assumption allows us to include the peak of the rotation curve for most of these galaxies and in the case that the peak happens well within 10 kpc the correction would be almost negligible since we would be measuring rotation in the flat regime. Additionally, truncating the baryons at a radius of 10 kpc allows us to directly calculate the correction to the circular velocity at that radius without having to make more complicated assumptions about the distribution of baryonic matter in galaxies, i.e., exponential lengths and Sérsic indices of disks and bulges and possibly extended gas and stellar halos.

To obtain the circular velocity measured at 10 kpc (V_{10}) for the Bolshoi DM halos, we need to use dark matter profiles and find the dark matter mass inside a 10 kpc radius. To do this, we could use the individual profile of each halo. However, once we select halos with given maximum circular velocity, individual halo-to-halo variations are small at 10 kpc. (The situation is different if we select halos with given virial mass. Then large deviations in concentrations result in large variations in V_{10} .) This is why instead of individual profiles we construct average profiles for halos with a narrow range $\Delta \log_{10} V \approx 0.05$ of maximum circular velocity.

We first bin and average the circular velocity profiles of the distinct halos found by the BDM code. These profiles are calculated for each halo (including unbound particles) in logarithmic radial bins in units of R_{vir} . Using distinct halos is convenient because it gives us density profiles that are less affected by interactions than those of subhalos. For the inner profiles of subhalos the effect is relatively small because the stripping happens preferentially at the outer radii. Using the averaged binned circular velocity profiles we obtain the velocity at 10 kpc. Within about 1.2% of the virial radius, discreteness effects render the profiles unreliable and we use instead extrapolation with the shape of a simple power-law in radius. For halos with $V_{\text{circ}} < 100 \text{ km s}^{-1}$ the full extent of the profiles suffer from measurement noise which we

avoid by extrapolating from the profile of halos with $\sim 100 \text{ km s}^{-1}$. Figure 3 shows the obtained median relation between V_{circ} and V_{10} for the Bolshoi DM halos without inclusion of the baryons.

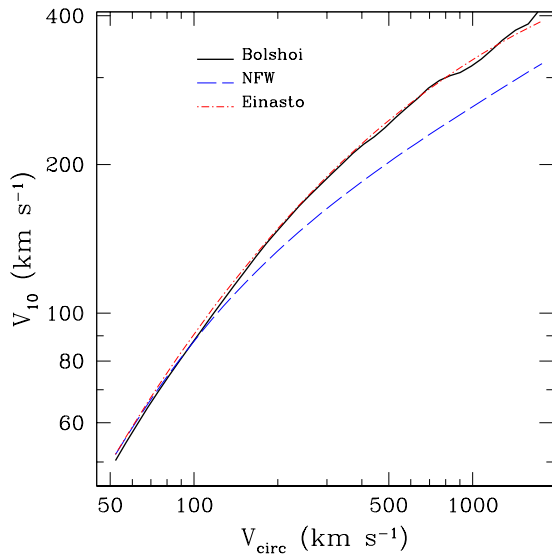


Fig. 3.— Relation between maximum circular velocity and the circular velocity measured at 10 kpc for the dark matter halo only (without including the baryon component). The solid curve shows the binned median values of the Bolshoi DM halo sample. The other curves show the relation obtained assuming the NFW (dashed) and the Einasto (dot-dashed) profiles with the halo concentration given by eq. (5).

The estimates of the relations obtained when a parametric form of the density profile is used are also shown for the case of the NFW (Navarro et al. 1997)

$$\rho(r) = \frac{4\rho_s}{(r/r_s)(1+r/r_s)^2}, \quad (3)$$

and the Einasto (Einasto 1965; Graham et al. 2006) universal profiles

$$\rho(r) = \rho_s \exp \left\{ -2n \left[(r/r_s)^{1/n} - 1 \right] \right\}; \quad (4)$$

where r_s is the radius at which the logarithmic slope of the density profile is -2 . Following Graham et al. (2006), we use $n = 6.0$. The concentration parameter defined for both models as $c \equiv R_{\text{vir}}/r_s$, is given by the relations obtained in

Paper I for distinct halos (Klypin et al. 2010):

$$c = 9.35 \left(\frac{M_{\text{vir}}}{10^{12} h^{-1} M_{\odot}} \right)^{-0.09}, \quad (5)$$

and

$$M_{\text{vir}} = \left(\frac{V_{\text{circ}}}{2.8 \times 10^{-2} \text{ km s}^{-1}} \right)^{3.16} h^{-1} M_{\odot}. \quad (6)$$

Note that in Figure 3 we use total dynamical masses and do not account for the condensation of baryons. For $V_{\text{circ}} = 100 - 450 \text{ km s}^{-1}$ the rotation (or density) profiles of the Bolshoi simulation are extremely well approximated by the Einasto parameterization, whereas NFW underestimates V_{10} by almost 20% at 450 km s^{-1} . Following the conclusions of Navarro et al. (2004) and Graham et al. (2006), we assume the Einasto profile when extrapolating the inner parts of the largest ($V_{\text{circ}} > 450 \text{ km s}^{-1}$) halos.

5.2. Adiabatic contraction of DM halos

Dissipation allows the baryons to condense into galaxies in the central regions of DM halos dragging the surrounding dark matter into a new more concentrated equilibrium configuration. If the density of the DM halo increases considerably within the extent of the disk, the peak circular velocity could be much larger than our previous estimates. There are different approximations for the adiabatic compression of the dark matter. Blumenthal et al. (1986) provide a simple analytical expression, which is known to overpredict the effect. The approximation proposed by Gnedin et al. (2004) predicts significantly smaller increase in the density of the dark matter. More recent simulations indicate even smaller compression (Tissera et al. 2009; Duffy et al. 2010). However, at a 10 kpc radius the dark matter contributes a relatively large fraction of mass even for large galaxies. As a result, the difference between the strong compression model of Blumenthal et al. (1986) and no-compression is only 10–20% in velocity.

We use the standard adiabatic contraction (AC) model of Blumenthal et al. (1986) to bracket the possible effect. We thus assume that following the condensation of the baryons, the dark matter particles adjust the radius of their orbits while

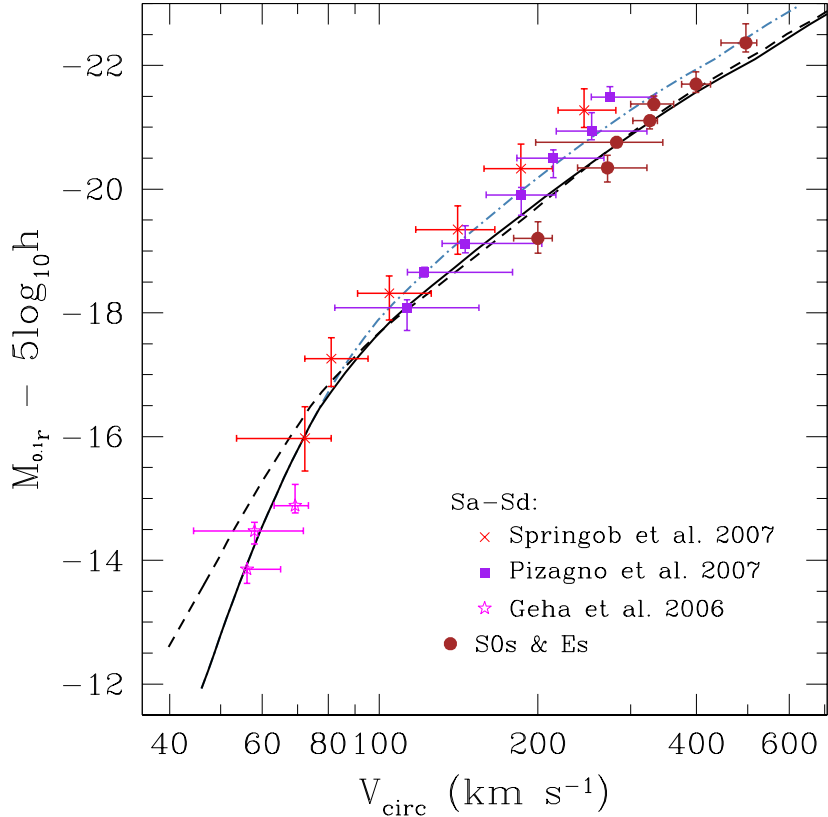


Fig. 4.— Comparison of the observed Luminosity-Velocity relation with the predictions of the Λ CDM model. The solid curve shows the median values of ${}^{0.1}r$ -band luminosity vs. circular velocity for the model galaxy sample. The circular velocity for each model galaxy is based on the peak circular velocity of its host halo over its entire history, measured at a distance of 10 kpc from the center including the cold baryonic mass and the standard correction due to adiabatic halo contraction. The dashed curve show results for a steeper ($\alpha = -1.34$) slope of the LF. The dot-dashed curve shows predictions after adding the baryon mass but without adiabatic contraction. Points show representative observational samples.

conserving angular momentum in the process. We solve the equation

$$M_{\text{tot}}(r_i)r_i = [M_{\text{DM}}(r_i)(1 - f_{\text{bar}}) + M_{\text{bar}}(r_f)]r_f, \quad (7)$$

where $r_f = 10$ kpc, $M_{\text{bar}}(r_f)$ is the total baryonic mass assigned to each halo and $f_{\text{bar}} = \Omega_{\text{bar}}/\Omega_{\text{matter}}$ is the universal fraction of baryons. We solve equation (7) for r_i and then add the dark matter mass $M_{\text{DM}}(r_i)(1 - f_{\text{bar}})$ to the mass of baryons to find the circular velocity. Note that this implies that only “cold baryons” (stars and cold gas) are left in the central regions of the galaxy, while the remaining hot baryons are at

larger radii. As expected, only the halos that are dominated by baryons at their centers suffer a significant increase in their measured circular velocities due to the increase in concentration of dark matter as result of adiabatic contraction.

6. Results

6.1. The Luminosity-Velocity relation

Figure 4 shows the predicted LV relation for galaxies in the Λ CDM model using the abundance-matching technique. The observational samples described in Section 2 are also

shown for comparison. The full curve in this plot shows results obtained using the Montero-Dorta & Prada (2009) LF of galaxies in the SDSS DR6 sample. It uses the adiabatic contraction model of Blumenthal et al. (1986). Predictions without the adiabatic contraction (with baryon contribution added in quadrature) are shown as the dot-dashed curve. The dashed curve shows the effect of a steeper slope at the faint end of LF that accounts for potential surface brightness incompleteness. (For details see Section 5). Although the dwarf sample studied by Geha et al. (2006) seems to agree better with a model using the Montero-Dorta & Prada (2009) LF, the scatter of the observed dwarf TF relation is so large that both LFs used in conjunction with the abundance of DM halos produce results that are consistent with the available data.

One may note that the AC model misses late-type points with $V_{\text{circ}} = 150 - 250 \text{ km s}^{-1}$ and the no-AC model practically goes through most of Pizagno et al. (2007) measurements. This should *not* be interpreted as either an advantage for the no-AC model or a disadvantage for the AC model. Our predictions are for the average population of all different types of galaxies. Because of the dichotomy of the LV diagram, a model that goes through either early type galaxies or through the late-type galaxies is a wrong model. The correct answer is a model, which tends to be close to spirals at low luminosities (where spirals dominate) and gradually slides to the ellipticals at the high-luminosity tail where elliptical dominate. It seems that the AC model tries to do exactly that, but it overshoots at the very bright tail of the LV relation.²

One also should not overestimate the quality of the observations. The fact that in Figure 4 the models are below the observational points at $V_{\text{circ}} = 90 - 110 \text{ km s}^{-1}$ is not a problem because of uncertainties in the observational data. For example, one of the data points of Blanton et al. (2008) in Figure 2 is at $V_{\text{circ}} = 100 \text{ km s}^{-1}$ and it is just below the models. There is also a systematic $\sim 10\%$ velocity offset between measurements of Pizagno et al. (2007) and Springob et al. (2007), which seems to indicate the current uncer-

²Schulz et al. (2009) find observational evidence for AC in elliptical galaxies.

tainties in the LV relation.

Considering the current level of the uncertainties, our model galaxies show remarkable agreement with observations spanning an order of magnitude in circular velocity and more than three orders of magnitude in luminosity. For galaxies above 200 km s^{-1} , our model produces results that agree extremely well with the observed luminosities of early-types (Es and S0s). Given how simple the prescription is, it is perhaps surprising how closely we can reproduce the observed properties of real galaxies. For galaxies with $V_{\text{circ}} = 100 - 200 \text{ km s}^{-1}$, DM halos without any corrections already occupy the region expected for galaxies. Corrections improve the fits, but it is important to emphasize that the abundance matching method yields the correct normalization of the LV relation regardless of the details of the corrections we implement. The shallow faint-end slope of the luminosity function causes the luminosity of dwarf halos to drop rapidly. Even though our model galaxies in this regime are slightly underluminous as compared with a simple power-law extrapolation from brighter galaxies, the dwarfs from the sample of Geha et al. (2006) seem to predict a deviation from a power-law TF in the same general direction.

The way it was constructed, our model galaxy sample does not include the variance in either the halo velocity function or in the galaxy luminosity function. This produces an LV relation with only very small scatter. In the present work we do not intend to reproduce or analyze the scatter found in the observations and we deal only with the medians of the distributions. The scatter we obtain is artificial and solely due to the fact that the luminosity assignment was done using the historical maximum circular velocity of the host halos (V_{acc}), typically its value at the moment of accretion, instead of the $z = 0$ value.

We now discuss in greater detail the results individual steps explained in Section 5.

6.2. The Luminosity-Velocity relation: different effects

6.2.1. Measuring circular velocity at 10 kpc

Observations do not always provide measurements of the circular velocity at 10 kpc. This is especially true for dwarf galaxies where the last

measured point of the rotation curve can be at 3–5 kpc. What are the errors associated with using measurements at different radii? Figure 5 presents three typical examples of the circular velocities expected for galaxies with vastly different masses.

The top panel shows a giant elliptical galaxy with $1.5 \times 10^{11} M_{\odot}$ of stellar mass distributed according to a $R^{1/4}$ law with a half-light radius of 5.5 kpc. The stellar component is embedded in a dark matter halo with virial mass $M_{\text{vir}} = 10^{13} M_{\odot}$ and median concentration $c = 7$. The maximum circular velocity (310 km s $^{-1}$) of the halo is reached at 160 kpc. The middle panel shows a Milky Way-size halo with maximum circular velocity 190 km s $^{-1}$, virial mass $M_{\text{vir}} = 1.7 \times 10^{12} M_{\odot}$, and median concentration $c = 9$ for its mass. The baryonic component consists of a Hernquist bulge ($M_{\text{bulge}} = 10^{10} M_{\odot}$, half-mass radius $R_{\text{bulge}} = 1$ kpc) and an exponential disk ($M_{\text{disk}} = 5 \times 10^{10} M_{\odot}$, scale radius $R_{\text{disk}} = 3.5$ kpc). The bottom panel is for a dwarf galaxy with $M_{\text{vir}} = 7 \times 10^{10} M_{\odot}$, $c = 12$, $V_{\text{max}} = 65$ km s $^{-1}$. Its baryons have two exponential disks: one for stars and one for gas with the mass ratio of 1:4 and radii $R_{*} = 1.5$ kpc and $R_{\text{gas}} = 3.0$ kpc. The total mass of baryons is $M_{\text{bar}} = 3 \times 10^8 M_{\odot}$. When we include baryons, we assume that most of them were blown out from the models and the only baryons left are those mentioned above. The DM circular velocities are derived by multiplying the simulated halo $M(< r)$ by the factor $\Omega_{\text{DM}}/\Omega_{\text{matter}}$ where $\Omega_{\text{matter}} = \Omega_{\text{DM}} + \Omega_{\text{bar}}$. For models labeled “DM+Baryons” at each radius we simply add the mass of baryons and the mass of dark matter. Models “DM+Baryons+AC” include adiabatic compression of dark matter according to the prescription of Blumenthal et al. (1986). In all three cases we use the Einasto dark matter profiles eq. (4) with $n = 6$.

After adding the baryons the circular velocity profiles become rather flat in the inner 5–10 kpc regions of the galaxies implying that measurements of circular velocities anywhere in this region are accurate enough to provide the value of the circular velocity at 10 kpc.

There are some caveats in choosing 10 kpc as a fiducial radius for either extremely massive spirals or giant ellipticals. Considering the correlation between central surface brightness and disk

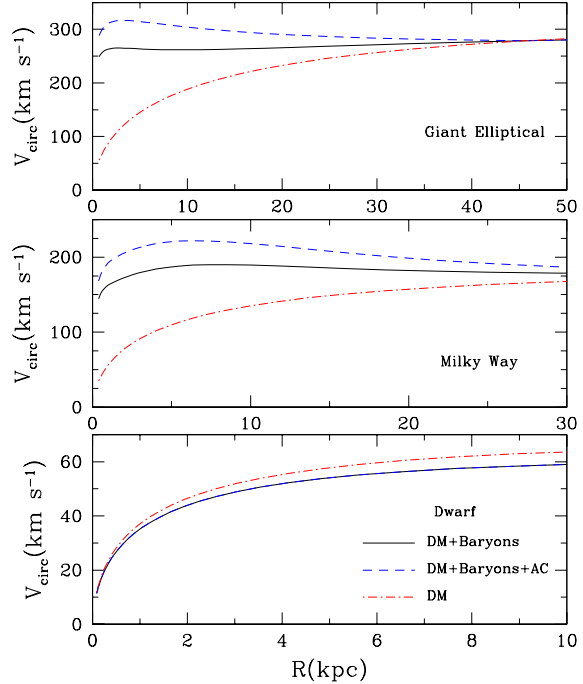


Fig. 5.— Effect of baryons on circular velocity profiles for three characteristic models of galaxies with virial masses $10^{13} M_{\odot}$ (top), $1.7 \times 10^{12} M_{\odot}$ (middle), and $7 \times 10^{10} M_{\odot}$ (bottom). Baryons are added to the dark matter in calculating the circular velocity (“DM+Baryons”). Effects of adiabatic compression of the dark matter are included in models “DM+Baryons+AC”. After adding the baryons the circular velocities are rather flat in the inner 5–10 kpc regions.

scale-length found by Courteau et al. (2007), the most luminous early-type galaxies appear to have scale-lengths as large as 15 kpc, whereas according to Courteau (1997) their rotation curves peak at about 1 scale-length. Hence, we may be *underestimating* the maximum observed rotation velocity of these systems in our sample. We may also *overestimate* circular velocities when we assume that most of the “cold” baryon mass is inside 10 kpc radius. In principle, some corrections can be applied to compensate this effect. However, our estimates show that at most this is a $\sim 20\%$ effect for spirals and somewhat smaller for ellipticals because they are more compact for the same luminosity. Considering existing uncertainties and complexities of implementing the correction, we decided not to use

them.

6.2.2. Dark matter profiles

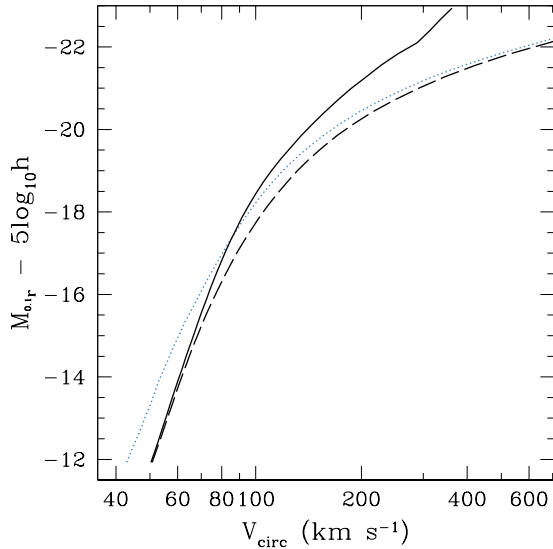


Fig. 6.— Comparison between different effects on the measured circular velocities of model galaxies without corrections for cold baryons or adiabatic contraction. The dotted curve shows the median $0.1r$ -band luminosity vs. circular velocity of the model galaxies that result from abundance matching using the maximum circular velocity of each DM halo at $z = 0$. The dashed line shows the effect of using the maximum value of the circular velocity *over the history of each halo* (V_{acc}). The solid curve shows the result of measuring V_{acc} for each halo at 10 kpc from the center. This affects intermediate and large halos the most since their circular velocity profile is still rising at that distance.

To estimate the effect of tidal stripping, Figure 6 shows the results (dashed curve) obtained when the luminosity assignment is performed using the maximum historical value of each halo's circular velocity V_{acc} and compares them with those for the $z = 0$ maximum circular velocity (dotted curve). For each halo the circular velocity estimated at $z = 0$ is smaller than its maximum historical value V_{acc} . This is why the dashed curve is to the right from the dotted one. If we compare luminosities at the same circular velocity, the differences can be substantial: almost one magnitude

for galaxies with $V_{\text{circ}} = 50 - 60 \text{ km s}^{-1}$. This is due to a steep decline of the LV relation for the dwarfs. The differences in velocities are much smaller. It mostly affects dwarf galaxies, underestimating their circular velocities by a maximum of $\sim 20\%$. For larger galaxies the effect of neglecting evolution decreases to less than 5%. This is mostly due to the fact that stripping only affects subhalos and they comprise only about 20% of the total halo population. In addition, only the small number of subhalos which orbit close to their host halo's center get significantly stripped and experience substantial decline of their circular velocity.

Comparison of LV relations constructed using V_{acc} one with the maximum the circular velocity (the dashed curve in Figure 6) and another with velocities V_{acc} estimated at 10 kpc (the full curve) indicates that this affects the largest halos the most. For example, the V_{10} velocity is almost a factor of two smaller than V_{max} for the group-size halos presented in the plot. Taking the circular velocity at 10 kpc also makes the LV relation much less curved as compared with the maximum velocity. Below $\sim 80 \text{ km s}^{-1}$ the maximum circular velocity of the DM halo happens near or within 10 kpc. So, the curve does not shift in this regime.

6.2.3. Effects of baryons and adiabatic compression

Figure 7 shows how baryons change the circular velocity at a 10 kpc radius. Here we use two extreme approximations that bracket the effect. The first approximation assumes that there is no change in the distribution of the dark matter. All simulations so far indicate that there is some compression. Hence, the no compression approximation definitely underpredicts the circular velocity V_{10} . The second approximation uses the adiabatic compression of Blumenthal et al. (1986), which produces the largest increase in the density of the dark matter. (The full and dashed curves were already shown in Figure 4). There are some differences between the LV relations predicted by those approximations. However, the largest effect is just adding baryons in quadrature to the circular velocity of the dark matter. Adiabatic compression increases the circular velocity even further, but the effect is relatively minor because the fraction of cold baryons gets progressively smaller for larger galaxies. The amount of baryons used for

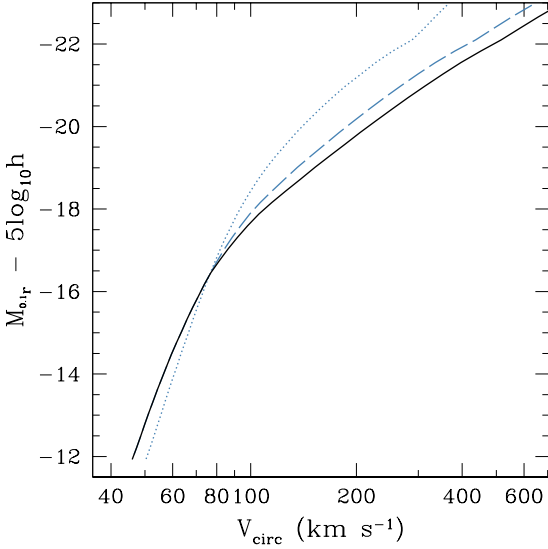


Fig. 7.— Effects of baryons on the LV relation. The dashed curve shows the circular velocity V_{10} after adding the baryon mass at the center of each halo without any adiabatic contraction of the dark matter. The solid curve shows the result of implementing the correction due to the adiabatic contraction of the halos (Blumenthal et al. 1986). For reference, the dotted line shows the circular velocity of the DM measured at 10 kpc (same as solid curve in Figure 6). Baryons have little effect on dwarfs ($V_{\text{circ}} < 100 \text{ km s}^{-1}$) since dwarfs are dominated by DM beyond a few kiloparsecs. Just adding the baryons in quadrature has the greatest effect with the adiabatic compression giving a 10-15% correction for bright galaxies.

the models is crucial for this test. As we discuss in §6.3, the abundance matching predicts relatively small cold baryon mass for dwarfs and giants, and this is why the adiabatic compression in Figures 5 and 7 is 10-20% at the most. Again, dwarfs below $\sim 80 \text{ km s}^{-1}$ are insensitive to the baryon presence. Here the full curve (DM+baryons) is slightly to the left from the DM-only curve because the latter includes a cosmological fraction of baryons, most of which are assumed to be blown out from the galaxies.

Figure 8 shows the LV relation for the case when we assume instead that half of all baryons within the virial radius or equivalently 8% of the

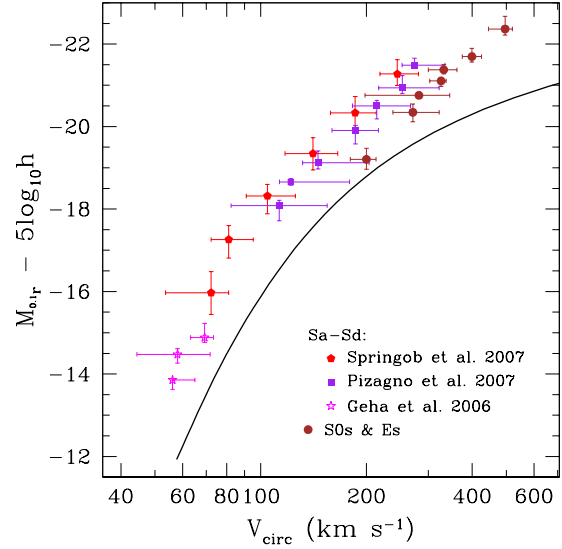


Fig. 8.— Effect of excessive mass of baryons. We assume that *half* of the universal baryon fraction within each halo forms its galaxy. Median values (solid curve) and 1- σ scatter (dashed curves) of $^{0.1}r$ -band luminosity vs. circular velocity of our model galaxies measured at 10 kpc from the center and including the correction due to adiabatic halo contraction. The same observational data shown in Figure 4 is reproduced here for comparison. The model systematically predicts too concentrated galaxies and fails to fit the observations.

virial mass are retained and are used to build the central galaxy. (Luminosity is not affected). Clearly, it is difficult to obtain the observed LV relation assuming a constant baryon fraction in the framework of the Λ CDM cosmology.

6.3. Baryon fraction and baryonic Tully-Fisher relation

For the LV relation the baryons played an ancillary role: they provided a correction to the circular velocity at 10 kpc. The correction is small for galaxies below 100 km s^{-1} . For large galaxies the baryons contribution increases and typically is about half of the mass. Regardless of their role in the LV relation, baryons are one of the prime subjects for the theory of galaxy formation. Unfortunately, accurate measurements of baryons are also prone to some uncertainties. Dynamical mea-

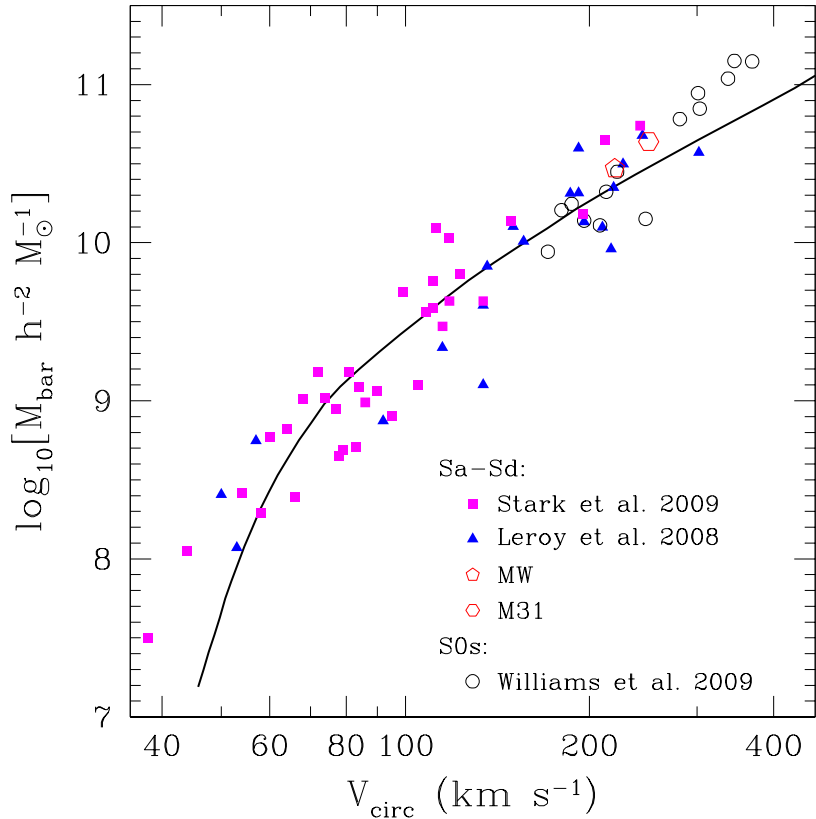


Fig. 10.— Mass of baryons as a function of circular velocity. The solid curve shows median values for the Λ CDM model. The total baryonic mass includes stars and cold gas and the circular velocity is measured at 10 kpc from the center while including the effect of adiabatic contraction. For comparison we show the individual galaxies of several galaxy samples. Intermediate mass galaxies such as the Milky Way and M31 lie very close to our model results.

surements of the baryonic component are difficult because of the dark matter-baryon degeneracies (e.g., Dehnen & Binney 1998). In other words, the baryon mass depends on what is assumed about the dark matter. Population synthesis provides an independent estimate of the stellar mass, but it has its share of complexities including the uncertainty in the initial mass function. Nevertheless, this is the best method available and, when possible, we use results of stellar population synthesis.

The baryonic Tully-Fisher relation (BTF) is one way of displaying results on the amount of “cold” baryons (stellar mass plus cold gas) in galaxies. The BTF relation was investigated over the years (McGaugh et al. 2000; Bell & de Jong 2001;

Verheijen 2001; McGaugh 2005; McGaugh et al. 2010). Here we use the recent observational samples of Stark et al. (2009) and Leroy et al. (2008). Stark et al. (2009) select gas-dominated spiral galaxies, which makes the results much less sensitive to the uncertainties in the IMF. We use their data obtained using the Kroupa IMF, which is close to the Chabrier (2003) IMF used by Li & White (2009). Leroy et al. (2008) present results based on the HI Nearby Galaxy Survey (THINGS): Walter et al. (2008). Measurement of luminosities in other bands including the infrared *Spitzer* measurements make reliable estimates of the stellar masses. Again, we use results for the Kroupa IMF. We also use the results of mass modeling of the Milky Way and M31 (Klypin et al.

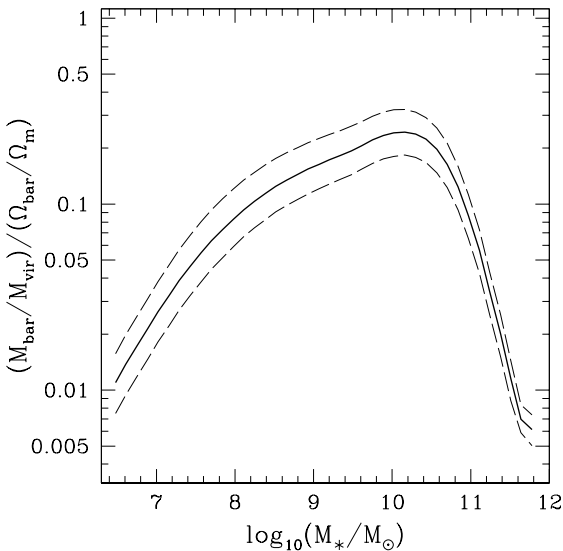


Fig. 9.— Baryon fraction relative to the universal value as a function of stellar mass for the Λ CDM model using the abundance-matching procedure. The solid lines show the median and 1σ scatter of the distribution, which is due to the scatter in halo concentrations.

2002; Widrow & Dubinski 2005).

The baryon fraction relative to the universal value as a function of stellar mass for the Λ CDM model using the abundance-matching procedure is shown in Figure 9. The baryon fraction f_b peaks at ≈ 0.2 for the stellar masses typical for Milky-Way-type galaxies and sharply falls on both sides of the mass spectrum. Our results are broadly consistent with Guo et al. (2010). We note that even the peak of $f_b \approx 0.2$ is almost twice smaller than what a few years ago was considered a fiducial value (Mo et al. 1998).

The baryonic Tully-Fisher relation is shown in Figure 10. Theoretical estimates from abundance matching provide a reasonable fit to observational results for galaxies ranging from dwarfs $V_{\text{circ}} \approx 50 \text{ km s}^{-1}$ to giants $V_{\text{circ}} \approx 300 \text{ km s}^{-1}$. There is a hint that observations show more baryonic mass for dwarfs below $V_{\text{circ}} = 50 \text{ km s}^{-1}$. It is not clear whether this is a real problem because of two uncertainties. First, there are observational issues. Statistics is one of them. Second, there is an uncertainty of the low-luminosity tail of the

luminosity function. Results of abundance matching are sensitive to the number-density of galaxies with absolute magnitudes $M_r > -14$, which are poorly constrained.

6.4. Galaxy Circular Velocity Function

Projecting the distribution of galaxies in the LV plane onto the luminosity axis produces the luminosity function, while projecting onto the circular velocity axis yields the circular velocity function (VF) of galaxies: the number-density of galaxies with given circular velocity. From a theoretical cosmology point of view, the VF is an ideal characterisation because it does not include uncertain predictions for the luminosity and require relatively modest corrections for mass of baryons. Unfortunately, it is more difficult to get it from observations and so far, there were only few attempts to do so (Gonzalez et al. 2000; Kochanek & White 2001; Chae 2010; Zavala et al. 2009; Zwaan et al. 2010).

For the theory the starting point is the velocity function of dark matter halos (e.g., Klypin et al. 2010). For halos with $V_{\text{circ}} < 500 \text{ km s}^{-1}$ it is well approximated by a power-law $n(> V_{\text{circ}}) \propto V_{\text{circ}}^{-\alpha}$, where $\alpha \approx 3$. This is for velocities taken at the maximum of circular velocity curves. Results must be corrected to V_{10} and to the effects of baryons.

The most recent measurement of the VF of nearby late-type galaxies was obtained by Zwaan et al. (2010). Their result is based on the blind HI sample of the HIPASS survey and is said to be complete down to $M_{\text{HI}} = 5.5 \times 10^7 M_\odot$ to a distance of 5 Mpc. Since gas-rich galaxies are thought to dominate at the low mass end, their sample should give an accurate measurement of the abundance of dwarfs if these galaxies contain enough neutral gas to be detected. To obtain a galaxy velocity function of all morphological types we also include the determination of the early-type VF done by Chae (2010), using the conversion between velocity dispersion and circular velocity found in Zwaan et al. (2010). Even though their VF was obtained indirectly using the observed relation between luminosity and stellar velocity dispersion, it agrees with previous direct measurements.

Figure 11 shows the results, as well as the modified Schechter fit to the VF of late-type galax-

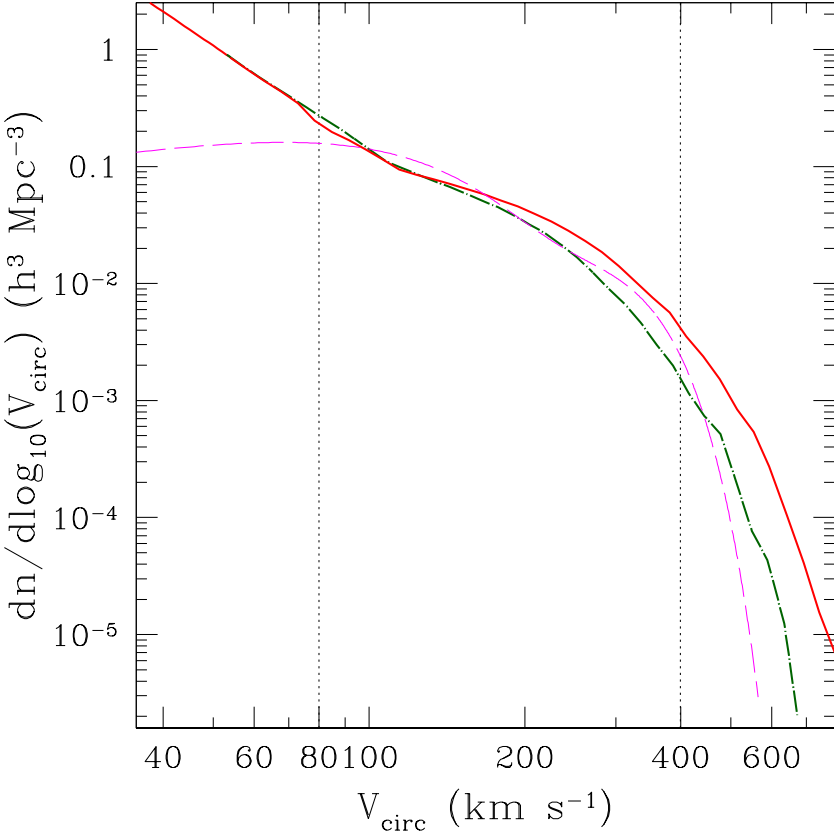


Fig. 11.— Comparison of theoretical (dot-dashed and thick solid curves) and observational (dashed curve) circular velocity functions. The dot-dashed line shows the effect of adding the baryons (stellar and cold gas components) to the central region of each DM halo and measuring the circular velocity at 10 kpc. The thick solid line is the distribution obtained when the adiabatic contraction of the DM halos is considered. Because of uncertainties in the AC models, realistic theoretical predictions should lie between the dot-dashed and solid curves. Both the theory and observations are highly uncertain for rare galaxies with $V_{\text{circ}} > 400 \text{ km s}^{-1}$. Two vertical dotted lines divide the VF into three domains: $V_{\text{circ}} > 400 \text{ km s}^{-1}$ with large observational and theoretical uncertainties; $< 80 \text{ km s}^{-1} < V_{\text{circ}} < 400 \text{ km s}^{-1}$ with a reasonable agreement, and $V_{\text{circ}} < 80 \text{ km s}^{-1}$, where the theory significantly overpredicts the number of dwarfs.

ies (Zwaan et al. 2010) and the fit for early-types found in Chae (2010). At intermediate to large masses ($80 < V_{\text{circ}} < 400 \text{ km s}^{-1}$), where the completeness of the surveys is hard to question, the VF of our model sample reproduces the observed abundances reasonably well. The abundance of MW-type galaxies is predicted to within 50% when adiabatic contraction is taken into account, and within a few percent when no contraction takes place. From our earlier analysis of the LV relation in Section 6 we are led to believe the effect

of AC is needed in order to obtain the correct position of elliptical and S0 galaxies in the plot. A more detailed treatment of AC might be necessary in order to better match the abundance of galaxies larger than the Milky Way. Our model galaxy VF overestimates the abundance of the most massive and rarest galaxies with $V_{\text{circ}} > 400 \text{ km s}^{-1}$ regardless of whether or not we implement the correction for contraction of the halos. Most of these extremely bright galaxies inhabit the centers of clusters, where it is very likely that the

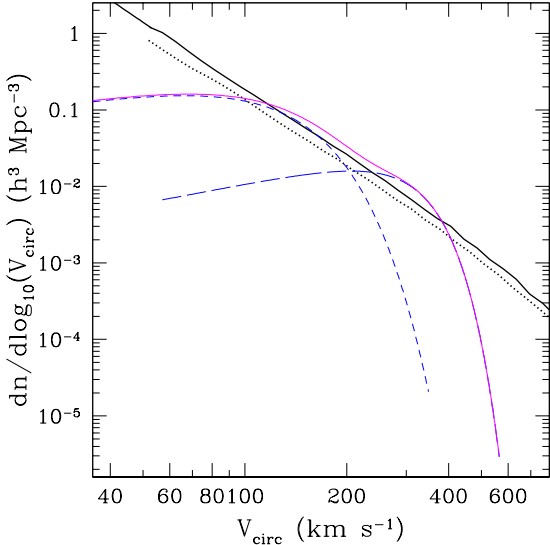


Fig. 12.— Details of the velocity function. The dotted line corresponds to the dark matter halo VF at $z = 0$, while the thick solid line shows the distribution of galaxies obtained if the maximum rotation velocity of the halos is measured at its historical maximum (i.e. before accretion). Note that the total mass includes 17% baryons that behave like dark matter in dissipationless simulations. The short (long) dashed curve shows the Schechter fit for late (early) type galaxies. The thin full curve is the total observed VF.

simplistic observational estimate of V_{circ} is breaking down. At small velocities ($V_{\text{circ}} < 80 \text{ km s}^{-1}$) the theory significantly overpredicts the number of dwarfs (Tikhonov & Klypin 2009; Zavala et al. 2009; Zwaan et al. 2010).

To illustrate the effect that each of the steps in our procedure has on the VF, we show in Figure 12 the VF of DM halos only. It also shows that when the stripping due to the merger history of each halo is considered, the halo VF does a slightly better job at matching the abundance of galaxies.

As we previously noted, the corrections due to the presence of the baryonic disk affect dwarfs ($V_{\text{circ}} < 100 \text{ km s}^{-1}$) very little and this effectively produces no shift in their abundance compared to that of their host halos at the low-mass end of the VF in Figure 11. This can be interpreted to

show that the dwarf overabundance problem cannot be resolved if both the LV relation and the VF of dwarf galaxies are to be reproduced at the same time. In other words, these galaxies must undergo a process that limits their abundance without changing their dynamical mass. The first possible origin for the large discrepancy between our model galaxies and the HIPASS VF could be observational bias. HIPASS is a blind HI survey and does not detect gas-poor galaxies. Only if gas-poor dwarf spheroidals dominate the galaxy population below $\sim 100 \text{ km s}^{-1}$ would it be possible to reconcile our results with the survey. This is highly unlikely since this type of galaxies are only a small fraction of the total dwarf population. On the other hand, if the HIPASS HI mass detection limit ($5.5 \times 10^7 M_{\odot}$ at 5 Mpc) is relatively high at the distances where most of their sample is found, incompleteness effects might explain the discrepancy.

Assuming that the surveys are complete, a possible solution to the problem is a mapping of *all* the dwarf galaxies below 50 km s^{-1} to DM halos in the range $50 - 100 \text{ km s}^{-1}$. This in turn implies that the measured rotation curves of a large fraction of dwarfs must severely underestimate the true maximum circular velocities of these galaxies. The only possible explanation for this bias would be that the optical and HI disk is truncated well inside the radius where the rotation curve flattens out.

Another scenario where the missing dwarfs are recovered requires most of them to have very low surface brightness. They would lie under the surface brightness limit of most surveys but this implies that they must have extremely extended disks with large scale-lengths to produce the optical luminosities required by their position in the LV relation.

7. Comparison with other results

Our results are broadly consistent with Guo et al. (2010), who also use the abundance matching technique. Specifically, in their Figure 6 they show the stellar-mass – circular velocity relation. The theoretical velocities appear to be *smaller* than the observed circular velocities for $V_{\text{circ}} = 100 - 150 \text{ km s}^{-1}$. Though Guo et al. (2010) did not apply necessary corrections dis-

cussed in our paper, they argue that inclusion of baryon mass may bring the theory into agreement with the observations. As we show, indeed this is the case.

Dutton et al. (2007) argue that the standard cosmological model with adiabatic contraction and standard concentrations fails to reproduce the observed LV relation. They also state that models with lower concentrations will be unable to match the luminosity function. Both conclusions are not compatible with our results. A number of assumptions made in Dutton et al. (2007) are either outdated or need corrections. For example, for their fiducial models they use the “standard concentrations” of Bullock et al. (2001), which were based on a simulation with $\sigma_8 = 1.0$, although they attempted to rescale them to a cosmological model with the normalization $\sigma_8 = 0.9$. The normalization of the current Λ CDM cosmological model is $\sigma_8 = 0.82$ based on CMB and other data (e.g. Jarosik et al. 2010), which results in halo concentrations that are $\sim 30\%$ lower than what Dutton et al. (2007) used. In turn, this reduces the dark matter circular velocities in inner regions of halo by about 15%. Fiducial models in Dutton et al. (2007) used the stellar masses found with the assumption of the scaled-down Salpeter IMF, which overestimates the masses by 0.15 dex (1.4 times) as compared with the Chabrier IMF used in our paper and in Li & White (2009). Some of the corrections were discussed by Dutton et al. (2007) and it was shown that they substantially improve the fit of the TF relation. However, the main difference is in the treatment of the LV relation. Dutton et al. (2007) used only late-type galaxies, while we also consider the early-types. At the bright end of the LV relation, the early-type galaxies dominate, and they substantially deviate from the spiral galaxies. The theoretical predictions for the average population should not go through the few rare spiral galaxies at the tip of the LV-relation.

Gnedin et al. (2007) studied structural properties of spiral galaxies and compared them with theoretical predictions. They also used Bullock et al. (2001) high concentrations as the “standard” model. It was concluded that the theory has problems and that adiabatic contraction is the likely culprit. Another possible solution was to lower the halo concentrations. Indeed, when

Gnedin et al. (2007) used concentrations for a model with $\sigma_8 = 0.74$ as predicted by simple theoretical arguments, they found that the theory gives an acceptable fit to the data. The problem is that $\sigma_8 = 0.74$ is too low. However, it appears that their analytical scaling with σ_8 was not accurate enough: the concentrations *actually used* by Gnedin et al. (2007) are practically (within 3%) the same as what we find in N-body simulations for the Bolshoi Λ CDM model with $\sigma_8 = 0.82$ (Klypin et al. 2010). In short, there seems to be no contradiction between our results and Gnedin et al. (2007) even when we consider models with standard adiabatic contraction. More definite conclusions require careful analysis and changes in the fraction of baryons among other things.

8. Discussion and Conclusions

In this paper we address one of the most difficult problems in cosmology: is the standard cosmological model Λ CDM compatible with observations when it comes to the prediction of the abundance and properties of galaxies? Instead of focusing on traditional issues such as the zero-point and the slope of the Tully-Fisher relation for spiral galaxies, we work with a more generic Luminosity-Velocity (LV) relation: a correlation of galaxy luminosity with the circular velocity at 10 kpc radius. We also investigate the baryonic mass - velocity relation, which following tradition we call the baryonic Tully-Fisher (BTF) relation, and the velocity function of galaxies. All these statistics are for galaxies of different types - from dwarf galaxies to normal spirals to giant ellipticals. These statistics – in combination with the theoretical predictions of the cosmic microwave background and the abundance and properties of dark matter halos and with properties of clustering of galaxies – are the main tests for validity of the Λ CDM model.

We use the abundance matching technique to assign luminosities to halos predicted by cosmological simulations. We also use abundance matching to assign stellar and baryonic masses. We find that all three statistics – LV, BTF, and velocity function – provide reasonably good fits to observations for galaxies ranging over 10 magnitudes in luminosity and for velocities from 50 km s^{-1} to

400 km s⁻¹. By construction, our models fit the observed luminosity and stellar mass functions. Since they are based on the Bolshoi simulation (Klypin et al. 2010), they also fit known properties of dark matter halos including the halo mass function and the dependence of halo concentration on mass. Previous publications (Conroy et al. 2006; Guo et al. 2010) showed that abundance matching also gives the correct clustering properties of galaxies. In short, *we have a model, that fits – at least on average – all basic statistics of galaxies with $V_{\text{circ}} > 50$ km s⁻¹ considered on ~ 10 kpc scale.*

Matching theory with observations requires a careful consideration of many different effects and application of different corrections. These effects were considered both for observations and for the theory. On the observational side, we compiled a representative sample of galaxies with measured circular velocities. Velocities were either asymptotic values (“flat part” of rotation curves) for spirals or measurements at ~ 10 kpc radius for S0s and Es. We do not use fits (such as power-law) to the data and simply plot the raw data. We do not apply morphological corrections of the TF relation (e.g., differences between Sb and Sa galaxies) because those corrupt the bright end of the LV relation. Since the Tully-Fisher luminosities are corrected to face-on, we de-correct the magnitudes of galaxies for the internal absorption to make them consistent with the measurement of the luminosity function.

For the theoretical predictions, we try to make all possible corrections to mimic the observational situation. For example, we do not use virial masses of halos because virial radii are too large as compared with the typical distances at which rotational velocities of real galaxies are measured. We do not assume a particular shape of density profiles: they are taken from simulations. Simulations required for this type of analysis should have a very high resolution so that subhalos are also resolved. This allows us to avoid using intermediate steps such as the Halo Occupation Distribution or the Conditional Luminosity Function, which are often applied to low-resolution simulations. The Bolshoi cosmological simulation (Klypin et al. 2010) provides high quality results resolving distinct halos and subhalos down to the completeness limit of $V_{\text{circ}} = 50$ km s⁻¹.

In summary, after applying all the corrections the abundance matching technique provides a reasonably good match for *median properties* of galaxies observed in the Universe. Different statistics have different accuracy. The LV relation is the most accurate because it is easier to measure luminosities than to estimate stellar masses, which require additional modeling and assumptions. This is why we consider the LV relation as our prime target. The Velocity Function is the least reliable. Observations are still at the very early stages. The completeness of the HIPASS VF is very uncertain. Just the fact that the detection limit is quoted at 5 Mpc tells that the accuracy of the HI mass function is not very high. This is why we treat the results on VF for $V_{\text{circ}} > 80$ km s⁻¹ as a “pass” for the theory in spite of some deviations such as at 130 km s⁻¹. More accurate treatment of these gas-rich galaxies may also change the situation: after all, changes in abundances and velocities by $\sim 10\%$ may (or may not) resolve the situation.

It is more difficult to reconcile the theory and observations at smaller velocities. Indeed, at $V_{\text{circ}} = 50$ km s⁻¹ the formal disagreement is almost a factor of ten. This is the only serious problem that we find when matching galaxies with dark matter halos. A similar problem on somewhat smaller scales was reported by Tikhonov & Klypin (2009), who studied the population of dwarfs in the ~ 10 Mpc region centered on the Milky Way galaxy. Tikhonov et al. (2009) argue that Warm Dark matter may be the solution to the problem.

In the present paper we did not attempt to model the spread in the LV and BTF relations. Our predictions are for median values and our prescription does not provide any natural spread of either LV or BTF relations. Just as in other publications on this subject (e.g., Dutton et al. 2007; Gnedin et al. 2007; Behroozi et al. 2010), we could have assumed some specific sources for the spread. For example, the spread in halo concentration may serve as a source of the spread in the LV relation. However, this is not more than an assumption: we substitute one unknown uncertainty (in LV relation) with another unknown uncertainty (how dark matter mass fluctuates in central regions of galaxies). In order to see this more clearly, let’s assume that the contribution of the dark matter to the rotation velocity of a galaxy depends on the maximum circular velocity

of the halos (not on their virial mass). This is definitely a better assumption, but it removes the uncertainty related with the concentration. The fraction of “cold” baryons is another possible factor. In this case we would need to know how the fraction varies from halo to halo. With our current state of cosmological simulations, we do not really know how to make this prediction.

In addition to being speculative, the source of the spread has another serious complication. Deviations from the observed median relations seems to have a systematic component: early-type galaxies are systematically below the median LV relation and gas-rich spirals are above it. It seems likely that the LV relation – like the color-magnitude diagram – has a bimodal structure. In this case, no simple random spread can explain the whole diagram. However uncertain, the spread must be explained. One approach might be to match halos separately to red and blue galaxies, for example using local density as well as luminosity. Ultimately it will be necessary to find the real source of the dynamical bimodality and to measure it observationally.

Abundance matching is a very successful way to make predictions how on the average galaxies can inhabit dark matter halos. It gives up solving the most difficult and the most important problem: how galaxies form inside dark matter halos. It simply assumes that the stellar mass and luminosity monotonically scale with the circular velocity. Bluntly speaking, it assumes that the maximum circular velocity of a halo determines the properties of the galaxy hosted by that halo. Remarkably, this can reproduce some basic environmental relations such as the morphology-density relation and the dependence of galaxy clustering on the luminosity of galaxies (e.g., Conroy et al. 2006) because of the correlation of environment with the average halo mass (Sheth et al. 2001; Sheth & Tormen 2004). However, there are potential issues with abundance matching. It is not clear how it can explain dependencies on environment even if galaxies are selected with the same *r*-band luminosity or the same stellar mass (Hogg et al. 2004; van der Wel 2008). There are also some internal inconsistencies. In the present form it assumes that *r*-band magnitude 100% correlates with the stellar mass, which may be problematic in detail. Modeling of the bimodality

in the LV relation (the apparent differences between early and late type galaxies) is another problem to address. It will be interesting to see how much better the results will be from more sophisticated abundance matching including galaxy color, local density, and scatter – as, e.g., in Tasitsiomi et al. (2004) – and from semi-analytic modeling based on the Bolshoi simulation. This work is in progress.

Here is a short summary of our results:

- In combination with previous results, we conclude that the standard Λ CDM model can reasonably well simultaneously explain the main global statistics of galaxies: the Luminosity Function, the stellar mass function, the Luminosity-Velocity relation, the baryonic mass - velocity relation, the abundance of galaxies with circular velocities with $V_{\text{circ}} > 80 \text{ km s}^{-1}$, and the clustering properties of galaxies of different magnitudes.
- There are systematic deviations in the LV relation with S0 and E’s galaxies being below spirals in the LV relation. With the current prescription we cannot explain those deviations.
- There seems to be an overabundance by a factor of ~ 10 of dwarf galaxies with $V_{\text{circ}} < 50 \text{ km s}^{-1}$. This is a serious problem for the theory: galaxies with these circular velocities cannot be affected much by “normal” physical processes (e.g., supernovae feedback or reionization of the Universe) proposed for the solution of the satellite problem. However, observational results on the abundance of dwarf galaxies still need to be improved.

We thank A. Dutton, T. Davis, F. Prada, R. Wechsler, A. Kravtsov, and M. Williams for helpful conversations, and M. Williams for providing his data in advance of publication. We acknowledge support of NSF grants at NMSU and NASA grants at UCSC. Our simulations and analysis were done using NASA Advanced Supercomputing (NAS) resources at NASA Ames Research Center. AJR was supported by National Science Foundation Grants AST-0808099 and AST-0909237.

REFERENCES

Agertz, O., Teyssier, R., & Moore, B. 2010, arXiv:1004.0005

Baldry, I. K., Glazebrook, K., & Driver, S. P. 2008, MNRAS, 388, 945

Behroozi, P. S., Conroy, C., & Wechsler, R. H. 2010, arXiv:1001.0015

Bell, E. F., & de Jong, R. S. 2001, ApJ, 550, 212

Benson, A. J., Bower, R. G., Frenk, C. S., Lacey, C. G., Baugh, C. M., & Cole, S. 2003, ApJ, 599, 38

Benson, A. J., & Bower, R. G. 2010, arXiv:1003.0011

Blanton, M. R., et al. 2003, ApJ, 594, 186

Blanton, M. R., et al. 2003, AJ, 125, 2348

Blanton, M. R., Lupton, R. H., Schlegel, D. J., Strauss, M. A., Brinkmann, J., Fukugita, M., & Loveday, J. 2005, ApJ, 631, 208

Blanton, M. R., & Roweis, S. 2007, AJ, 133, 734

Blanton, M. R., Geha, M., & West, A. A. 2008, ApJ, 682, 861

Blumenthal, G. R., Faber, S. M., Flores, R., & Primack, J. R. 1986, ApJ, 301, 27

Boylan-Kolchin, M., Springel, V., White, S. D. M., Jenkins, A., & Lemson, G. 2009, MNRAS, 398, 1150 (MS-II)

Bullock, J. S., Kravtsov, A. V., & Weinberg, D. H. 2000, ApJ, 539, 517

Bullock, J. S., Kolatt, T. S., Sigad, Y., Somerville, R. S., Kravtsov, A. V., Klypin, A. A., Primack, J. R., & Dekel, A. 2001, MNRAS, 321, 559

Chae, K.-H. 2010, MNRAS, 402, 2031

Chabrier, G. 2003, PASP, 115, 763

Cole, S., Aragon-Salamanca, A., Frenk, C. S., Navarro, J. F., & Zepf, S. E. 1994, MNRAS, 271, 781

Cole, S., Lacey, C. G., Baugh, C. M., & Frenk, C. S. 2000, MNRAS, 319, 168

Conroy, C., Wechsler, R. H., & Kravtsov, A. V. 2006, ApJ, 647, 201

Conroy, C., & Wechsler, R. H. 2009, ApJ, 696, 620

Courteau, S. 1997, AJ, 114, 2402

Courteau, S., Dutton, A. A., van den Bosch, F. C., MacArthur, L. A., Dekel, A., McIntosh, D. H., & Dale, D. A. 2007, ApJ, 671, 203

de Blok, W. J. G., & McGaugh, S. S. 1997, MNRAS, 290, 533

de Blok, W. J. G. 2010, Advances in Astronomy, 2010

de Vaucouleurs, G., de Vaucouleurs, A., Corwin, H. G., Jr., Buta, R. J., Paturel, G., & Fouque, P. 1991, Volume 1-3, XII, 2069 pp. 7 figs.. Springer-Verlag Berlin Heidelberg New York

Dehnen, W., & Binney, J. 1998, MNRAS, 294, 429

de Lorenzi, F., Gerhard, O., Saglia, R. P., Sambhus, N., Debattista, V. P., Pannella, M., & Méndez, R. H. 2008, MNRAS, 385, 1729

de Lorenzi, F., et al. 2009, MNRAS, 395, 76

Duffy, A. R., Schaye, J., Kay, S. T., Dalla Vecchia, C., Battye, R. A., & Booth, C. M. 2010, arXiv:1001.3447

Dunkley, J., et al. 2009, ApJS, 180, 306

Dutton, A. A., van den Bosch, F. C., Dekel, A., & Courteau, S. 2007, ApJ, 654, 27

Einasto, J. 1965, Trudy Inst. Astrofiz. Alma-Ata, 5, 87

Eke, V. R., Navarro, J. F., & Steinmetz, M. 2001, ApJ, 554, 114

Faber, S. M., & Jackson, R. E. 1976, ApJ, 204, 668

Flores, R. A., & Primack, J. R. 1996, ApJ, 457, L5

Forestell, A., & Gebhardt, K. 2010, ApJ, in press, arXiv:0803.3626

Fukugita, M., Hogan, C. J., & Peebles, P. J. E. 1998, ApJ, 503, 518

Fukugita, M., & Peebles, P. J. E. 2004, *ApJ*, 616, 643

Geha, M., Blanton, M. R., Masjedi, M., & West, A. A. 2006, *ApJ*, 653, 240

Gnedin, O. Y., Kravtsov, A. V., Klypin, A. A., & Nagai, D. 2004, *ApJ*, 616, 16

Gnedin, O. Y., Weinberg, D. H., Pizagno, J., Prada, F., & Rix, H.-W. 2007, *ApJ*, 671, 1115

Gonzalez, A. H., Williams, K. A., Bullock, J. S., Kolatt, T. S., & Primack, J. R. 2000, *ApJ*, 528, 145

Gottloeber, S., & Klypin, A. 2008, in "High Performance Computing in Science and Engineering Garching/Munich 2007", Eds. S. Wagner et al, Springer, Berlin 2008 (arXiv:0803.4343)

Governato, F., Willman, B., Mayer, L., Brooks, A., Stinson, G., Valenzuela, O., Wadsley, J., & Quinn, T. 2007, *MNRAS*, 374, 1479

Governato, F., et al. 2010, *Nature*, 463, 203

Graham, A. W., Driver, S. P., Petrosian, V., Conselice, C. J., Bershady, M. A., Crawford, S. M., & Goto, T. 2005, *AJ*, 130, 1535

Graham, A. W., Merritt, D., Moore, B., Diemand, J., & Terzić, B. 2006, *AJ*, 132, 2701

Guo, Q., White, S., Li, C., & Boylan-Kolchin, M. 2010, *MNRAS*, 367

Hill, D. T., Driver, S. P., Cameron, E., Cross, N., Liske, J., & Robotham, A. 2010, arXiv:1002.3788

Hinshaw, G., et al. 2009, *ApJS*, 180, 225

Hogg, D. W., et al. 2004, *ApJ*, 601, L29

Humphrey, P. J., & Buote, D. A. 2010, *MNRAS*, 403, 2143

Jarosik, N., et al. 2010, arXiv:1001.4744

Jensen, J. B., Tonry, J. L., Barris, B. J., Thompson, R. I., Liu, M. C., Rieke, M. J., Ajhar, E. A., & Blakeslee, J. P. 2003, *ApJ*, 583, 712

Kauffmann, G., White, S. D. M., & Guiderdoni, B. 1993, *MNRAS*, 264, 201

Klypin, A., & Holtzman, J. 1997, arXiv:astro-ph/9712217

Klypin, A., Gottlöber, S., Kravtsov, A. V., & Khokhlov, A. M. 1999, *ApJ*, 516, 530

Klypin, A., Kravtsov, A. V., Bullock, J. S., & Primack, J. R. 2001, *ApJ*, 554, 903

Klypin, A., Zhao, H., & Somerville, R. S. 2002, *ApJ*, 573, 597

Klypin, A., Valenzuela, O., Colín, P., & Quinn, T. 2009, *MNRAS*, 398, 1027

Klypin, A., Trujillo-Gomez, S., & Primack, J. 2010, arXiv:1002.3660

Kochanek, C. S., & White, M. 2001, *ApJ*, 559, 531

Komatsu, E., et al. 2009, *ApJS*, 180, 330

Komatsu, E., et al. 2010, arXiv:1001.4538

Kravtsov, A. V., Klypin, A. A., & Khokhlov, A. M. 1997, *ApJS*, 111, 73

Kravtsov, A. V. 1999, Ph.D. Thesis

Kravtsov, A. V., Berlind, A. A., Wechsler, R. H., Klypin, A. A., Gottlöber, S., Allgood, B., & Primack, J. R. 2004, *ApJ*, 609, 35

Lauer, T. R., et al. 2007, *ApJ*, 662, 808

Leroy, A. K., Walter, F., Brinks, E., Bigiel, F., de Blok, W. J. G., Madore, B., & Thornley, M. D. 2008, *AJ*, 136, 2782

Li, C., & White, S. D. M. 2009, *MNRAS*, 398, 2177

Lupton, R. 2005, <http://www.sdss.org/dr7/algorithms/sdssUBVRITransform.html>

Macciò, A. V., Kang, X., Fontanot, F., Somerville, R. S., Koposov, S., & Monaco, P. 2010, *MNRAS*, 402, 1995

Mandelbaum, R., Seljak, U., Kauffmann, G., Hirata, C. M., & Brinkmann, J. 2006, *MNRAS*, 368, 715

Maraston, C. 2005, *MNRAS*, 362, 799

Masters, K. L., Springob, C. M., & Huchra, J. P. 2008, *AJ*, 135, 1738

McGaugh, S. S., Schombert, J. M., Bothun, G. D., & de Blok, W. J. G. 2000, *ApJ*, 533, L99

McGaugh, S. S. 2005, *ApJ*, 632, 859

McGaugh, S. S., Schombert, J. M., de Blok, W. J. G., & Zagursky, M. J. 2010, *ApJ*, 708, L14

Mo, H. J., Mao, S., & White, S. D. M. 1998, *MNRAS*, 295, 319

Mo, H. J., Mao, S., & White, S. D. M. 1998, *MNRAS*, 295, 319

Montero-Dorta, A. D., & Prada, F. 2009, *MNRAS*, 399, 1106

Moore, B. 1994, *Nature*, 370, 629

Moore, B., Ghigna, S., Governato, F., Lake, G., Quinn, T., Stadel, J., & Tozzi, P. 1999, *ApJ*, 524, L19

Nagino, R., & Matsushita, K. 2009, *A&A*, 501, 157

Napolitano, N. R., et al. 2009, *MNRAS*, 393, 329

Navarro, J. F., Frenk, C. S., & White, S. D. M. 1997, *ApJ*, 490, 493

Navarro, J. F., & Steinmetz, M. 2000, *ApJ*, 538, 477

Navarro, J. F., et al. 2004, *MNRAS*, 349, 1039

O'Sullivan, E., & Ponman, T. J. 2004, *MNRAS*, 354, 935

O'Sullivan, E., Sanderson, A. J. R., & Ponman, T. J. 2007, *MNRAS*, 380, 1409

Paturel, G., Petit, C., Prugniel, P., Theureau, G., Rousseau, J., Brouty, M., Dubois, P., & Cambrésy, L. 2003, *A&A*, 412, 45

Peletier, R. F., Davies, R. L., Illingworth, G. D., Davis, L. E., & Cawson, M. 1990, *AJ*, 100, 1091

Pizagno, J., et al. 2007, *AJ*, 134, 945

Primack, J. R. 2009, *New Journal of Physics*, 11, 105029

Romanowsky, A. J., & Kochanek, C. S. 2001, *ApJ*, 553, 722

Romanowsky, A. J., Douglas, N. G., Arnaboldi, M., Kuijken, K., Merrifield, M. R., Napolitano, N. R., Capaccioli, M., & Freeman, K. C. 2003, *Science*, 301, 1696

Rozo, E., et al. 2009, *ApJ*, 699, 768

Sakai, S., et al. 2000, *ApJ*, 529, 698

Sansom, A. E., O'Sullivan, E., Forbes, D. A., Proctor, R. N., & Davis, D. S. 2006, *MNRAS*, 370, 1541

Schulz, A. E., Mandelbaum, R., & Padmanabhan, N. 2009, arXiv:0911.2260

Sheth, R. K., Mo, H. J., & Tormen, G. 2001, *MNRAS*, 323, 1

Sheth, R. K., & Tormen, G. 2004, *MNRAS*, 350, 1385

Somerville, R. S., & Primack, J. R. 1999, *MNRAS*, 310, 1087

Springel, V., et al. 2005, *Nature*, 435, 629 (MS-I)

Springob, C. M., Masters, K. L., Haynes, M. P., Giovanelli, R., & Marinoni, C. 2007, *ApJS*, 172, 599

Stark, D. V., McGaugh, S. S., & Swaters, R. A. 2009, *AJ*, 138, 392

Strauss, M. A., et al. 2002, *AJ*, 124, 1810

Tasitsiomi, A., Kravtsov, A. V., Wechsler, R. H., & Primack, J. R. 2004, *ApJ*, 614, 533

Tikhonov, A. V., & Klypin, A. 2009, *MNRAS*, 395, 1915

Tikhonov, A. V., Gottlöber, S., Yepes, G., & Hoffman, Y. 2009, *MNRAS*, 399, 1611

Tissera, P. B., White, S. D. M., Pedrosa, S., & Scannapieco, C. 2009, arXiv:0911.2316

Tully, R. B., & Fisher, J. R. 1977, *A&A*, 54, 661

van der Wel, A. 2008, *ApJ*, 675, L13

Vale, A., & Ostriker, J. P. 2004, *MNRAS*, 353, 189

Valenzuela, O., Rhee, G., Klypin, A., Governato, F., Stinson, G., Quinn, T., & Wadsley, J. 2007, *ApJ*, 657, 773

Verheijen, M. A. W. 2001, *ApJ*, 563, 694

van der Wel, A. 2008, *ApJ*, 675, L13

Walter, F., Brinks, E., de Blok, W. J. G., Bigiel, F., Kennicutt, R. C., Thornley, M. D., & Leroy, A. 2008, *AJ*, 136, 2563

Weijmans, A.-M., Krajnović, D., van de Ven, G., Oosterloo, T. A., Morganti, R., & de Zeeuw, P. T. 2008, *MNRAS*, 383, 1343

Widrow, L. M., & Dubinski, J. 2005, *ApJ*, 631, 838

Williams, M. J., Bureau, M., & Cappellari, M. 2009, *MNRAS*, 400, 1665

Willman, B., Governato, F., Dalcanton, J. J., Reed, D., & Quinn, T. 2004, *MNRAS*, 353, 639

York, D. G., et al. 2000, *AJ*, 120, 1579

Zavala, J., Jing, Y. P., Faltenbacher, A., Yepes, G., Hoffman, Y., Gottlöber, S., & Catinella, B. 2009, *ApJ*, 700, 1779

Zwaan, M. A., Meyer, M. J., & Staveley-Smith, L. 2010, *MNRAS*, 403, 1969